Check for updates

JGR Oceans

RESEARCH ARTICLE
10.1029/2021JC017417

Special Section:
Uncovering the hidden links between dynamics, chemical, biogeochemical and biological processes under the changing Arctic

Strong Margin Influence on the Arctic Ocean Barium Cycle Revealed by Pan-Arctic Synthesis

Laura M. Whitmore[1,2], Alan M. Shiller[1], Tristan J. Horner[3], Yang Xiang[4], Maureen E. Auro[3], Dorothea Bauch[5], Frank Dehairs[6], Phoebe J. Lam[4], Jingxuan Li[7], Maria T. Maldonado[7], Chantal Mears[8], Robert Newton[9], Angelica Pasqualini[10], Hélène Planquette[11], Robert Rember[12], and Helmuth Thomas[8]

[1]School of Ocean Science and Engineering, University of Southern Mississippi, Stennis Space Center, MS, USA, [2]Now at College of Fisheries and Ocean Sciences, University of Alaska Fairbanks, Fairbanks, AK, USA, [3]NIRVANA Laboratories, Woods Hole Oceanographic Institution, Woods Hole, MA, USA, [4]Department of Ocean Sciences, University of California, Santa Cruz, CA, USA, [5]GEOMAR Helmholtz Centre for Ocean Research, Kiel, Germany, [6]Department of Analytical, Environmental and Geochemistry, Vrije Universiteit Brussel, Brussels, Belgium, [7]Department of Earth Ocean & Atmospheric Sciences, University of British Columbia, Vancouver, BC, Canada, [8]Institute of Carbon Cycles, Helmholtz Centre Hereon, Geesthacht, Germany, [9]Lamont-Doherty Earth Observatory, Columbia University, New York, NY, USA, [10]Department of Earth and Environmental Engineering, Columbia University, New York, NY, USA, [11]University of Brest, CNRS, IRD, Ifremer, LEMAR, Plouzane, France, [12]International Arctic Research Center, University of Alaska Fairbanks, Fairbanks, AK, USA

Abstract Early studies revealed relationships between barium (Ba), particulate organic carbon and silicate, suggesting applications for Ba as a paleoproductivity tracer and as a tracer of modern ocean circulation. *But, what controls the distribution of barium (Ba) in the oceans?* Here, we investigated the Arctic Ocean Ba cycle through a one-of-a-kind data set containing dissolved (dBa), particulate (pBa), and stable isotope Ba ratio (δ^{138}Ba) data from four Arctic GEOTRACES expeditions conducted in 2015. We hypothesized that margins would be a substantial source of Ba to the Arctic Ocean water column. The dBa, pBa, and δ^{138}Ba distributions all suggest significant modification of inflowing Pacific seawater over the shelves, and the dBa mass balance implies that ~50% of the dBa inventory (upper 500 m of the Arctic water column) was supplied by nonconservative inputs. Calculated areal dBa fluxes are up to 10 μmol m^{-2} day^{-1} on the margin, which is comparable to fluxes described in other regions. Applying this approach to dBa data from the 1994 Arctic Ocean Survey yields similar results. The Canadian Arctic Archipelago did not appear to have a similar margin source; rather, the dBa distribution in this section is consistent with mixing of Arctic Ocean-derived waters and Baffin Bay-derived waters. Although we lack enough information to identify the specifics of the shelf sediment Ba source, we suspect that a sedimentary remineralization and terrigenous sources (e.g., submarine groundwater discharge or fluvial particles) are contributors.

Plain Language Summary We investigated the barium (Ba) cycle in the Arctic Ocean. The oceanic Ba cycle is supported by the interplay of seawater mixing, river inputs, sediment inputs, and particle formation and export from the water column. We determined that the distribution of dissolved Ba in the upper 500 m of the Arctic Ocean is largely set by a shelf sediment source; this is newly described, as previous literature assumed rivers and seawater mixing were the predominant contributors to the distribution. This discovery fits in with recent findings that the shelf sediments are a major source of radium and other trace metals to the surface Arctic Ocean. This is important to consider as the warming climate continues to erode Arctic ice cover (sea ice or glacial). Monitoring the relative sources of Ba to the water column can help define how warming impacts Arctic Ocean biogeochemistry.

Key Points:

- A mass balance approach indicates margin sources of barium (Ba) account for ~50% of the budget
- Amerasian Arctic Ocean samples exhibit inverted Ba isotope profiles, though still fall on the global array
- Particle supply from the shelves and dissolution in the deep Amerasian Arctic Ocean is a likely source of dissolved Ba

Supporting Information:

Supporting Information may be found in the online version of this article.

Correspondence to:

L. M. Whitmore and A. M. Shiller,
lmwhitmore@alaska.edu;
alan.shiller@usm.edu

Citation:

Whitmore, L. M., Shiller, A. M., Horner, T. J., Xiang, Y., Auro, M. E., Bauch, D., et al. (2022). Strong margin influence on the Arctic Ocean barium cycle revealed by pan-Arctic synthesis. *Journal of Geophysical Research: Oceans*, *127*, e2021JC017417. https://doi.org/10.1029/2021JC017417

Received 31 MAR 2021
Accepted 16 MAR 2022

Author Contributions:

Conceptualization: Laura M. Whitmore, Alan M. Shiller, Tristan J. Horner, Robert Rember
Data curation: Laura M. Whitmore, Tristan J. Horner, Yang Xiang, Maureen E. Auro, Dorothea Bauch, Frank Dehairs,

© 2022 The Authors.
This is an open access article under the terms of the Creative Commons Attribution-NonCommercial License, which permits use, distribution and reproduction in any medium, provided the original work is properly cited and is not used for commercial purposes.

1. Introduction

The Arctic sits at the forefront of global change, and we have already observed the manifestation of anthropogenic effects in the region (Wassmann et al., 2011). The Arctic Ocean is a particularly climate-relevant ocean basin due to the impact it has on the formation of North Atlantic Deep Water, which is a driver of the Atlantic Meridional Overturning Circulation, and also due to its impact on planetary albedo through sea-ice coverage. The distribution of heat and freshwater within the Arctic Ocean, which is determined by the relative contributions of different source waters, modulates deep water formation, sea-ice extent, and ecosystem functioning.

Jingxuan Li, Chantal Mears, Robert Newton, Angelica Pasqualini, Hélène Planquette, Robert Rember
Formal analysis: Laura M. Whitmore
Funding acquisition: Alan M. Shiller, Tristan J. Horner, Phoebe J. Lam, Maria T. Maldonado, Robert Newton, Hélène Planquette
Investigation: Laura M. Whitmore
Methodology: Alan M. Shiller, Tristan J. Horner, Yang Xiang, Jingxuan Li
Project Administration: Alan M. Shiller
Supervision: Alan M. Shiller
Writing – original draft: Laura M. Whitmore
Writing – review & editing: Laura M. Whitmore, Alan M. Shiller, Tristan J. Horner, Yang Xiang, Dorothea Bauch, Frank Dehairs, Phoebe J. Lam, Jingxuan Li, Chantal Mears, Robert Newton, Hélène Planquette

Geochemical tracers have played a central role in unraveling the distributions of water types within the Arctic Ocean, though nonconservative processes have often complicated interpretations (e.g., Whitmore et al., 2020 and references therein). Barium (Ba) is a widely applied tracer of biogeochemistry and has been used as a tracer of freshwater inputs (e.g., Guay et al., 2009), mixing (e.g., Hsieh & Henderson, 2017), and paleoceanographic conditions (e.g., Horner et al., 2021). The distribution of dissolved Ba (dBa) in the Arctic Ocean is unique in that high concentration, river-derived dBa can be observed in the surface (Guay et al., 2009; Guay & Falkner, 1997). Three decades of dBa data exist in the Arctic (e.g., Abrahamsen et al., 2009; Guay et al., 2009; Guay & Falkner, 1997; Taylor et al., 2003), which offers an opportunity to assess its distribution through time in the context of a changing Arctic. The stable isotope composition of dBa (δ^{138}Ba) is another means to assess the relative influence of sources and internal cycling on the dBa distribution. Oceanic dissolved δ^{138}Ba profiles are typically enriched in isotopically heavy Ba at the surface and depleted at depth; recent literature has unveiled the importance of mixing on this distribution (e.g., Bates et al., 2017; Horner et al., 2015; Hsieh & Henderson, 2017). Internal cycling of Ba has often complicated our understanding of Ba distributions. Following an empirical correlation between barite sinking flux and particulate organic carbon export flux (Dymond et al., 1992), pBa observations, in both the water column and sediments, has been applied as a proxy for productivity and carbon export (e.g., Dehairs et al., 1997, 1980; Dymond et al., 1992; Eagle et al., 2003). However, the mechanisms driving the barite-export relationship remain unclear (Cardinal et al., 2005; Chow & Goldberg, 1960; Dehairs et al., 1980; Ganeshram et al., 2003; Martinez-Ruiz et al., 2019), which makes application of the methodology empirical rather than mechanistic. In the central Arctic Ocean, productivity is low relative to other ocean basins and modern measurements of export are limited (Honjo et al., 2010 and references therein; Nöthig et al., 2020). Thus, examining the pBa distribution in the Arctic Ocean may shed light both on processes affecting the dBa distribution as well as the potential to apply modern and paleoceanographic Ba proxies for productivity and export.

Here, we comprehensively evaluate the Ba cycle in the Arctic by leveraging results from four synoptic expeditions conducted under the umbrella of GEOTRACES. Our study is guided by the overarching question: *what controls the Ba distribution in the Arctic Ocean?* A number of studies have assessed the viability of Ba as a fluvial source tracer in the Arctic Ocean (Abrahamsen et al., 2009; Alkire et al., 2015; Bolt, 2021; Guay et al., 2009; Roeske, Bauch, Rutgers van der Loeff, & Rabe, 2012); these studies make the assumption that dBa behaves conservatively. Few studies have attempted to quantify nonconservative behavior of dBa in the Arctic (Hendry et al., 2018; Roeske, Bauch, Rutgers van der Loeff, & Rabe, 2012; Taylor et al., 2003; Thomas et al., 2011), which limits its utility to a predominantly qualitative descriptor of freshwater sources. Additional studies on similar tracers have identified shelf sediments as a substantial portion of their geochemical budgets (e.g., Granger et al., 2018; Kipp et al., 2018). Thus, in this context, one goal of our work is to expand the scope of previous Ba studies to a pan-Arctic perspective to assess nonconservative Ba sources and sinks in the Arctic marine system.

We were able to determine the relative importance of the various source (seawater inflow, rivers, margins, and sea ice) and sink terms (burial of barite and water outflow) in the Arctic Ba budget, as well as consider the role of internal cycling (formation and dissolution of pBa), through a combination of dissolved and particulate Ba concentration data, analysis of δ^{138}Ba, and historical Ba data. Dissolved and particulate Ba data were sourced from four 2015 GEOTRACES expeditions (GN01 [USA], GN02/3 [CAN], and GN04 [EU]), dissolved Ba isotope data was from GN01 [USA], and historical Ba data included riverine data from the Arctic Great Rivers Observatory and an extensive pan-Arctic survey from 1994 (Guay & Falkner, 1997). We used three primary steady-state models: a $Ba_{anomaly}$ assessment to determine regions with nonconservative Ba excesses and deficits (Section 5.1), an isotope mass balance analysis to constrain the origin of Ba excesses (Section 5.2), and an upper Arctic Ocean box model to quantify the magnitude of non-conservative Ba sources and sinks (Section 5.3). Given the assumptions and uncertainties in each model, we assess the system through combination of the three approaches and consider recent literature to determine the relative importance of source and sink terms in the Ba budget. We discuss the likely mechanisms (authigenic or terrigenous sedimentary flux) by which the margins supply Ba to the Arctic (Section 5.4). These processes are important to identify and constrain to better predict whether anthropogenic climate change will fundamentally alter Arctic Ba inventories. We also investigated the origin of Ba in the deep Arctic Ocean (Section 5.5). This region is comparatively under-studied, particularly for trace metals, and we discuss probable pathways by which these waters accumulate Ba and attain their δ^{138}Ba. Such a discussion is important to have considering changing surface ocean conditions.

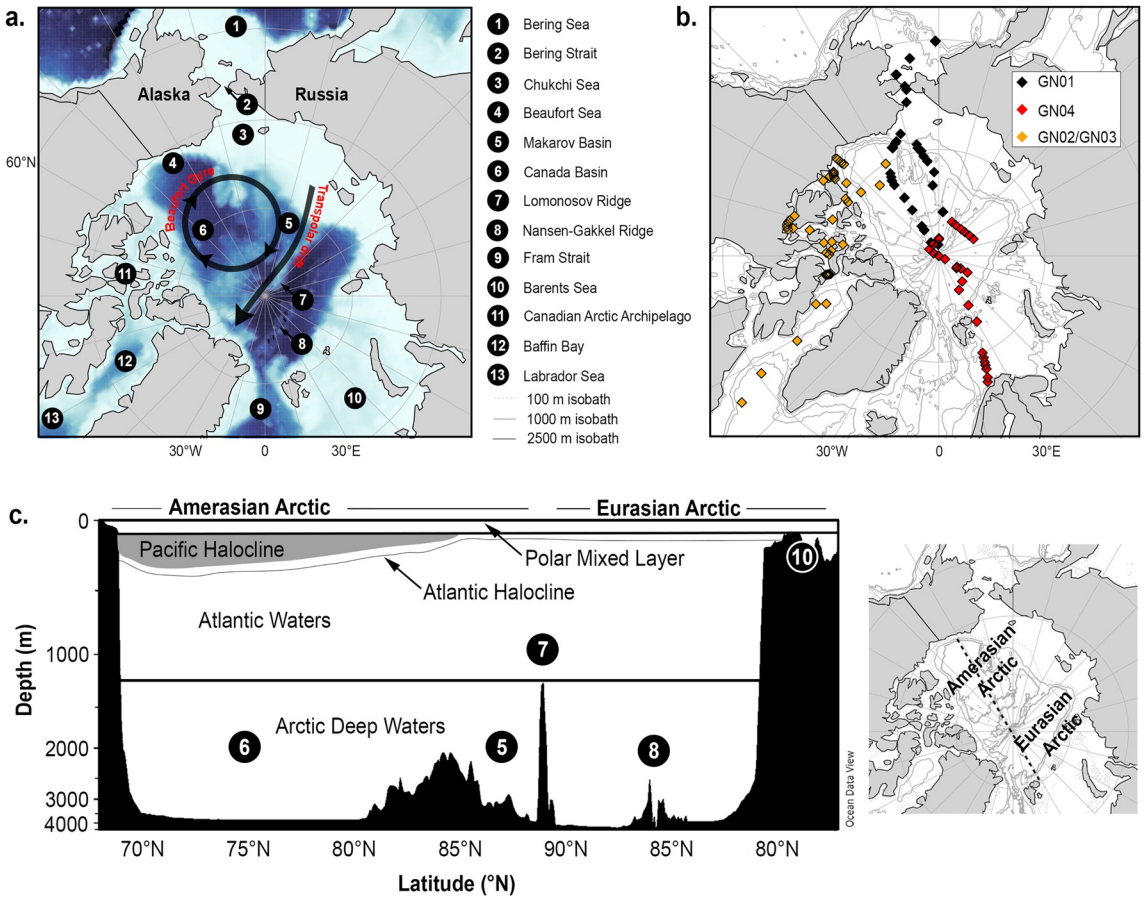

Figure 1. Regional geography, hydrography, and station map. (a) Local geographic features and predominant surface circulation. (b) Station map for the 2015 GEOTRACES expeditions. U.S. GEOTRACES (GN01) are black diamonds, European GEOTRACES (GN04) are red diamonds, and Canadian GEOTRACES (GN02 and GN03) are orange diamonds. (c) Regional hydrographic features, the small map to the right of panel c includes a section line (dashed) that indicates where the bathymetry for panel c is derived from, as well as labels for the Amerasian and Eurasian sectors of the Arctic Ocean (divided by the ridge feature in the central Arctic Ocean). Figure modified from Whitmore et al. (2019).

Lastly, we explore how Arctic dBa is exported to the global ocean (Section 5.6). The Canadian Archipelago is one of two pathways (Fram Strait is the other) by which waters exit the Arctic Ocean and thus this pathway offers an opportunity to assess whether (and how) Arctic modification of water masses is communicated to the North Atlantic Ocean.

2. The 2015 Arctic GEOTRACES Sections

Four oceanographic expeditions were conducted between July and October 2015 that encompassed the Amerasian and Eurasian sectors of the Arctic Ocean, and included shelf areas. such as the Bering Sea, Barents Sea, and Canadian Arctic Archipelago (Figure 1). The cruises were conducted within the framework of the international GEOTRACES program, which aims to characterize the distributions of trace elements and their isotopes. Cruises departed from the United States (GN01/HLY1502: August 9–12 October 2015), Norway (GN04/PS94: August 17–14 October 2015), and Canada (GN02 and GN03/ArcticNet 1502 and 1503: July 10–20 August 2015 and September 4–1 October 2015, respectively), and are referred to by their GEOTRACES cruise ID (GN0#) throughout the text.

GN01 transited through the Bering and Chukchi Seas to the North Pole and completed two transects: one in the Makarov Basin (180°W) and another in the Canada Basin (150°W). GN02 and GN03 completed surveys through the Canadian Arctic Archipelago, with a primary transect from the Canada Basin in the Amerasian Basin through Baffin Bay to the Labrador Sea (Figures 1a and 1b). GN02 and GN03 also conducted a high-resolution cross

section across Lancaster Sound (see Section 5.6). GN04 sampled a transect from the Barents Sea to the North Pole roughly along the 30°E longitudinal line (due to ice conditions, there are longitudinal variations in the transect). Additionally, GN04 completed a high resolution transect perpendicular to 135°E. Each cruise shared a crossover station and data from these stations were analyzed for quality control and intercalibration purposes (Text S3, Figure S2 and S3 in in Supporting Information S1). Sampling for all cruises occurred in late summer and sea ice extent was at roughly the annual minimum (Text S1 and Figure S1 in Supporting Information S1).

Throughout the article, we will refer to the key regions as the "Amerasian Basin," "central Arctic Ocean," "Eurasian Basin," and "Canadian Arctic Archipelago (CAA)." The Amerasian and Eurasian Basins are the North American and Eurasian sides of the Lomonosov Ridge, respectively (Figure 1c). The central Arctic Ocean is the region north of 85°N, which—during the 2015 expeditions—was influenced by Transpolar Drift waters (Charette et al., 2020; see Section 2.1 for further discussion on regional hydrography).

2.1. Regional Hydrography

Seawater enters the Arctic Ocean through the Bering Strait (Pacific-derived waters), the Fram Strait (Atlantic-derived) and the Barents Sea (Atlantic-derived). Substantial freshwater input to these regions sustains low salinity waters in the Arctic Ocean's mixed layer (Polar Mixed Layer; PML). The Arctic Ocean receives ~10% of global river discharge (e.g., McClelland et al., 2012; Milliman & Farnsworth, 2013), is surrounded by land with relatively small gateways for seawater exchange, and is the smallest ocean basin. River discharge contributes to the PML basin-wide. The combination of river discharge, sea ice melt, and Pacific-derived seawater ($S \sim 32.5$), yields a strong halocline expressed in the Amerasian Basin (Pacific Halocline; PH; Figure 1c). Pacific-derived waters undergo geochemical and physical modification due to exchange with shelf sediments, seasonal brine formation and sea ice melt, and particulate interactions and biological activity during transit on the regional shelves before entering the Arctic Ocean basins (e.g., Fransson et al., 2001; Gong & Pickart, 2016; Whitmore et al., 2019). Circulation of surface waters in the Amerasian Basin is set by the anticyclonic Beaufort Gyre and the Transpolar Drift (TPD); in the Eurasian Arctic Ocean, surface circulation is generally cyclonic. The TPD is a strong current that advects waters from the Chukchi, East Siberian, and Laptev Seas across the central Arctic Ocean (Charette et al., 2020 and references therein).

Transformations of physical properties imparted on Pacific-derived waters such as temperature (T) and salinity (S) result in the formation of warm, fresh Pacific summer water (PSW) and cold, salty Pacific winter water (PWW) that contribute to the PH (Gong & Pickart, 2016; Weingartner et al., 1998). Warm waters in the PH, principally summer Bering Strait Water (sBSW) or Alaska Coastal Water (ACW; Steele et al., 2004), are from warming that occurs over the shelf. We refer to the warm PH waters (sBSW and ACW) as "Pacific Summer Water" (PSW) following Timmermans et al. (2014). The PH has a residence time of roughly 10–15 yr (Kipp et al., 2019; Schlosser et al., 1999) and its distribution is sensitive to atmospheric conditions (e.g., Steele et al., 2004). The PH is predominantly observed in the Amerasian Arctic Ocean basins.

The "Atlantic halocline" or "lower halocline" lies directly below the PH and is likely composed of Atlantic-derived seawater that has similarly undergone modifications due to physical or biogeochemical processes occurring over the shelves (Coachman & Barnes, 1963; Rudels et al., 2004). Circulating below the halocline are Atlantic-derived "intermediate waters." Two distinct Atlantic-derived water masses have been identified with residence times of 20–30 yr (Kipp et al., 2019; Schlosser et al., 1999): Barents Sea Branch Water (BSBW) and Fram Strait Branch Water (FSBW; e.g., Schauer, 1995). Barents Sea Branch Waters cross the shallow Barents Sea shelf before entering the Nansen Basin through St. Anna Trough; the density of these waters increases through cooling and, over the deep central Arctic basins, they circulate beneath the FSBW (Rudels, 2018). Below the intermediate waters (>1,500 m), Arctic Deep Water circulates within each basin. The Lomonosov Ridge restricts flow between the deep Eurasian basins and the Amerasian basins (Talley et al., 2011). In the Amerasian Basin, the Canada and Makarov Basins are further divided by the Alpha-Mendeleev Ridge. As there are few outflow sites for deep waters, these waters have long residence times of ~150–500 yrs (Kipp et al., 2019; Schlosser et al., 1999; Tanhua et al., 2009). Arctic Deep Water geochemical signals may be influenced by near-slope mixing processes and brines (Bauch et al., 1995; Middag et al., 2009; Roeske, Rutgers van der Loeff, Middag, & Bakker, 2012; Rudels & Quadfasel, 1991).

Waters exiting the Arctic Ocean leave through both the Fram Strait and the Canadian Arctic Archipelago (CAA; Rudels, 2018) and ultimately contribute to North Atlantic Deep Water formation sites. Net volume fluxes out of the Fram Strait and the CAA (via Davis Strait) are roughly equivalent (~2 Sv each; Beszczynska-Möller et al., 2011). Our accounting of Ba fluxes exiting the Arctic focuses on the CAA due to data availability. The region is tidally influenced and winds play a role in setting surface currents (McLaughlin et al., 2004; Peterson et al., 2012). All waters entering the CAA must transit through one of several relatively shallow straits (<500 m) before entering the Labrador Sea (e.g., McLaughlin et al., 2004; Melling, 2000). Flow through the CAA is generally eastward and southward; however, some of the straits are wide enough for counter currents to form along the coastlines (see Section 5.6; LeBlond, 1980; McLaughlin et al., 2004).

Similar to Pacific-derived waters that transit over shelves, seawater passing through the CAA could be modified during that transit. For example, sediment exchange, biological activity, river input, and sea ice melt and formation may influence the geochemical composition of CAA waters. The estimated combined discharge of all CAA rivers is about 10% of the total river discharge into the Arctic (Alkire et al., 2017; Haine et al., 2015) which accounts for roughly 1% of waters flowing through the CAA. For this study, we focus on waters in the Parry Channel (see Section 5.7).

3. Methods

3.1. Sample Collection and Analysis

For all cruises, dBa samples were filtered and collected into acid cleaned HDPE bottles from a trace metal clean rosette following GEOTRACES protocols (Cutter et al., 2014). Specifics to each rosette can be accessed via the cruise reports (https://www.geotraces.org/category/scientific-publications/cruise-reports/). Sampling protocols for each lab group are further detailed in the Supplementary Material (Text S2–S4 in Supporting Information S1). Additionally, large and small fraction (>51 and 0.8–51 μm), particulate Ba (pBa), and aluminum (pAl) samples were collected via McLane Research in situ pumps (WTS-LV) during the GN01 section, also following GEOTRACES protocols (Cutter et al., 2014; Xiang & Lam, 2020); total particulate concentrations were determined as the sum of large and small fractions. Total particle distributions were sampled from GO-FLO bottles during GN02, GN03, and GN04. GN01 pump casts were set up as described in Xiang and Lam (2020). GN02/GN03 GO-FLO bottles were mounted to a standard trace metal clean rosette (Cutter et al., 2014) and GN04 GO-FLOs were mounted to the Titan sampling system (De Baar et al., 2008); trace metal clean bottle sampling procedures were followed (Cutter et al., 2014; Planquette & Sherrell, 2012).

3.1.1. Dissolved Ba Concentrations

Samples from GN01 were analyzed at the Center for Trace Analysis (University of Southern Mississippi; USM; Shiller & Horner, 2021). Samples from GN02/GN03 were analyzed at Vrije Universiteit Brussel (VUB; Thomas et al., 2021) and GN04 samples were analyzed at the University of Alaska, Fairbanks (UAF; Rember, 2018). All samples were analyzed by isotope dilution ICP-MS (inductively coupled plasma mass spectrometry) similar to the method of Jacquet et al. (2005). Details of each lab's methodology can be found in the supplemental information including an intercalibration comparison (Text S2–S5, Tables S1, S2, Figures S2 and S3 in Supporting Information S1). In general, all labs reported relative standard deviation (RSD) <2% and results at crossover stations suggest that inter-laboratory offsets were typically <2.5 nmol kg^{-1} (i.e., <6% of typical sample concentrations).

3.1.2. Dissolved Ba Isotopes

Dissolved Ba isotope measurements ($\delta^{138/134}$Ba; Shiller & Horner, 2021) were made on a subset of the GN01 samples at the NIRVANA Labs at Woods Hole Oceanographic Institution, including all shelf samples ($n = 23$), Bering Sea endmember samples ($n = 4$), slope samples ($n = 11$) and some Makarov and Canada Basin samples ($n = 20$). Analytical methods followed those described by Bates et al. (2017). Ba-isotopic analyses were performed using a ThermoFinnigan Neptune multiple collector ICP-MS situated at the WHOI Plasma Facility (see Text S3 in Supporting Information S1 for further detail). Sample isotopic composition was solved iteratively—with additional nested loops for isobaric corrections—and reported relative to the nearest four bracketing measurements of NIST standard reference material 3104a in delta-notation (Equation 1).

$$\delta^{138}Ba_{NIST}(‰) = \left(\frac{^{138/134}Ba_{sample}}{^{138/134}Ba_{NIST}} - 1\right) \times 1000. \quad (1)$$

All samples were analyzed between 2 and 8 times (median $n = 4$). Reported values represent the weighted mean of n measurements, whereby the weightings were assigned according to the inverse square of the corresponding measurement uncertainty. Uncertainties are reported as the greater of either the weighted uncertainty for n measurements (±2 *SE*, standard error), or our long-term precision of ±0.03‰ (±2 *SD*, standard deviation; Horner et al., 2015). Standard reference material and precision of analyses are reported in the Supplemental Material (Table S1 in Supporting Information S1).

3.1.3. Particulate Concentrations

Particle samples (pBa and pAl) were analyzed by ICP-MS at the UCSC Plasma Analytical Facility (GN01; Lam, 2020), at UBC (GN02/GN03), and Pôle Spectrométrie Océans/LEMAR (GN04). Particulate Ba concentrations were obtained via a refluxing digestion method (Cullen & Sherrell, 1999; Ohnemus et al., 2014; Planquette & Sherrell, 2012; Xiang & Lam, 2020). Filters (Supor) were digested by refluxing of the sample with a strong acid solution at high heat (e.g., HNO_3, HF, and/or HCl) followed by drying down of the acid mixture (Text S4 in Supporting Information S1). Final pBa and pAl sample solutions were analyzed in low and medium resolution, respectively. Indium (1 ppb) was used as an internal standard for ICP-MS analysis.

The lithogenic and non-lithogenic components of pBa are considered; we assume the non-lithogenic fraction represents authigenically formed barite (pBa_{xs}). This fraction is determined by subtracting from the total pBa, the lithogenic pBa which is estimated from the measured pAl multiplied by a lithogenic Ba:Al ratio (Equation 2; Jacquet et al., 2005). The terrigenous Ba:Al ratio may not be uniform across all Arctic continental sources. The bulk continental crust (BCC) Ba:Al ratio is roughly two times less than upper continental crust (UCC; e.g., Rudnick & Gao, 2014), in the basins this doubling makes little difference since non-lithogenic pBa accounts for ≥90% of total pBa. On the shelf, the selection in ratio causes more sensitivity in the predicted components (using BCC results in a larger non-lithogenic component). However, the selection of Ba:Al ratio does not impact our interpretations of the results; we, therefore, apply the terrigenous Ba:Al ratio (0.0015 mol:mol) of global upper continental crust (UCC) values that were reported by Rudnick and Gao (2014) as 628 μg Ba g^{-1} and 15.4% (wt) Al_2O_3.

$$pBa_{xs} = pBa_{obs} - \left(pAl_{obs} \times \frac{Ba_{UCC}}{Al_{UCC}} \right). \quad (2)$$

3.1.4. Ancillary Data

Ancillary data, such as salinity and temperature, were retrieved from public databases when possible, including BCO-DMO for GN01 (Cutter et al., 2019) and PANGAEA for GN04 (Ober et al., 2016). Water mass fractions for the Arctic Ocean basins were determined using a four-component linear mixing model. The four-component mixing model uses salinity (S), water oxygen isotopic composition ($\delta^{18}O$), and nitrate and phosphate to determine the fraction of Atlantic, Pacific, meteoric, or sea-ice derived waters in each sample. This method is outlined in greater detail in elsewhere (Text S6, Table S3 and Figure S4 in Supporting Information S1; Newton et al., 2013), but employs the relative N:P ratio differences between Atlantic and Pacific water as a tracer of each water type. Using nutrients in a water mass deconvolution relies on the assumption that the ratio of those nutrients behave conservatively, recent studies have demonstrated potential for other tracers to similarly deconvolve the water column (Andersson et al., 2008; Laukert et al., 2017; Whitmore et al., 2020). However, only nutrient data was available for all samples in the upper 500 m; therefore, we utilized the nutrient approach.

3.2. Data Analysis

The four cruises cover a large area of the Arctic Ocean. Given the good inter-laboratory agreement, we combined datasets from different cruises to produce three composite ocean sections that we refer to throughout this study. We defined two sections in the Arctic Ocean basins and one through the Canadian Arctic Archipelago. Section A includes stations in the Bering and Chukchi seas, the Makarov Basin (along the Alpha-Mendeleev Ridge) and into the Amundsen Basins (Figure 3a). Section B progresses from the Chukchi Sea shelf-break, through the Canada, Amundsen, and Nansen Basin and onto the Barents Sea Shelf (Figure 3b). Section C progresses from the Canada Basin, through the Canadian Arctic Archipelago, through Baffin Bay and ends south of Baffin Bay (Figure 3c). Section plots were generated using weighted-average gridding in Ocean Data View 5.1.5 (Schlitzer, 2018).

Table 1
Dissolved Ba Endmember Estimates (nmol kg^{-1})

	Minimum	Best estimate	Maximum
dBa_{met}	90	130[a]	190
dBa_{SIM}[b]	2	6.5	11
dBa_{Pac}	55	56	57
dBa_{Atl}[a]	39	42	45

[a]Guay et al.(2009). [b]Marsay et al.(2018).

In this study, we calculated "predicted" dissolved Ba (dBa_{pred}) to investigate the conservative behavior of dBa and δ^{138}Ba. Predicted dBa was calculated following Equation 3.

$$dBa_{pred} = dBa_{met} f_{met} + dBa_{ice} f_{ice} + dBa_{pac} f_{pac} + dBa_{atl} f_{atl}. \quad (3)$$

The four components identified in the subscripts of Equation 3 are: meteoric (met, representative of riverine component and precipitation), sea ice melt/formation (ice), Pacific-derived waters (pac), and Atlantic-derived waters (atl). The dBa of each endmember is weighted by the fraction (f) of the component to determine the predicted concentration of dBa (dBa_{pred}) in each sample. Ba endmembers for these components are described in Section 3.2.1 (Table 1) and the fractions were determined using a linear water mass deconvolution (Section 3.1.4).

The $Ba_{anomaly}$ (Equation 4) is the deviation of dBa from the predicted distributions. An anomaly value of 0 indicates that measured dBa matches predictions, implying conservative behavior. Ba excesses ($Ba_{anomaly} > 0$) indicate observed dBa concentrations higher than predicted, suggesting an additional source of Ba not accounted for in the mixing model. Deficits ($Ba_{anomaly} < 0$) indicate dBa removal relative to conservative behavior.

$$Ba_{anomaly} = dBa_{obs} - dBa_{pred}. \quad (4)$$

Saturation state, and saturation indices, are indicative of whether an ion pair is over -, under-, or perfectly saturated with respect to a solid phase comprising the same two ions. Barite saturation state is formulated (Equation 5) as the ratio of the ion activity product (of Ba and SO_4) and the solubility product constant (K_{sp}; Horner & Crockford, 2021; Millero, 1982; Monnin et al., 1999; Rushdi et al., 2000).

$$\Omega_{barite} = \frac{\{Ba\} \times \{SO_4\}}{K_{sp}}. \quad (5)$$

The surface ocean is generally undersaturated in respect to barite ($BaSO_4$; Monnin et al., 1999). Theoretical saturation occurs when the saturation state (Ω_{barite}) equals 1; however, realistically, Ba is at saturation at values near 1 (Monnin et al., 1999). Spontaneous nucleation of barite does not occur in solutions with $\Omega_{barite} < 8$ (Nancollas & Purdie, 1963) and the precipitation of barite is unlikely in the absence of organic matter-Ba interactions (Deng et al., 2019).

3.2.1. Determination of dBa Endmembers

Considering the prior literature and available data, we determined a minimum, best-estimate, and maximum dBa endmember concentrations for each water source in the Arctic (Table 1). The best-estimate endmember values may be considered "apparent" endmembers as they are the outcome of several sources that are considered regionally integrated or averaged.

For meteoric dBa, we combine annual flow weighted means (AFWM) of the major rivers to determine an Arctic-wide estimate and to consider the effects of estuarine processes. An average of the AFWMs from the seven major rivers represents our maximum estimate (190 nmol kg^{-1}; Holmes et al., 2018). This value does not incorporate estuarine processes (i.e., addition of dBa through desorption from particles) and it equally weights the contribution of each river to the entire Arctic Ocean. North American river water (>300 nmol kg^{-1}) is mainly diverted eastward toward the CAA and thus has less overall impact on the central Arctic than Eurasian Rivers (Guay & Falkner, 1997); thus, the mean of all AFWMs should bias the river Ba estimate high. Our "best-guess" estimate (130 nmol kg^{-1}) is from Guay et al. (2009) and considers both the AFWMs and previous estimates of the effective river endmember (i.e., includes estuarine processes). Our minimum estimate is an average of Eurasian river AFWMs; this is low because it does not include estuarine processes or any influence from North American rivers (Guay & Falkner, 1998; Kipp, Spall, et al., 2020).

We consider Station 4 from GN01 in the Bering Strait a representative Pacific Endmember (dBa_{pac}); dBa at the Bering Strait was 56 ± 1 nmol kg^{-1}. We recognize that Pacific derived waters have passed over the shallow Bering Sea shelf before reaching this point and compare this value to GN01 Station 1, on the slope of the Bering Sea (the Pacific-most station sampled). At GN01 Station 1 we observed dBa between 38.7 and 61.1 nmol kg^{-1} in

the upper 100 m. The Bering Strait average agrees with the 54 ± 5 nmol kg^{-1} reported "Pacific Endmember" by Guay et al. (2009). Note, dBa in the Bering Strait has been reported at higher concentrations (e.g., near bottom dBa > 100 nmol kg^{-1}; Falkner et al., 2013). However, the GN01 Station 1 profile does not exceed ~70 nmol kg^{-1} in the upper 300 m and Bering Sea basin and Gulf of Alaska surface dBa observations are ~50–60 nmol kg^{-1} (Yamamoto-Kawai et al., 2010). Thus, we attribute observations of high dBa on the shelves to sources of Ba to the shelf region (e.g., rivers, shelf sediments, and internal cycling).

No seawater entering the Arctic Ocean at the Fram Strait or Barents Sea gateways was sampled in this set of cruises. However, we approximate the Atlantic seawater endmember as the average Eurasian Basin samples between 200 and 500 m (40.1 ± 0.6 nmol kg^{-1}, $n = 30$); these waters are Atlantic-origin waters that have spent the least amount of time in the Arctic Ocean and can be identified by their warm temperature. This estimate is insignificantly different than a dBa_{Atl} endmember of 42 ± 3 nmol kg^{-1} as determined from and used in previous literature (Guay et al., 2009; Le Roy et al., 2018; Roeske, Bauch, Rutgers van der Loeff, & Rabe, 2012). We apply the literature estimate throughout our analyses and consider it to be more conservative.

Sea ice may be a source of Ba through sequestration of Ba into the sea-ice complex and release to the water column. Locally, annual sea ice formation and melt could have a net zero influence on the water column (Thomas et al., 2011). However, in consideration of the Arctic Ocean basins we must consider the possibility that the sea-ice formed over the shelves could melt in the basins and may, therefore, be a non-zero source of Ba to the basin water column. Importantly, the magnitude of this source and role of sea ice formation distributing dBa in the water column remains unclear (Hendry et al., 2018; Hoppema et al., 2010; Marsay et al., 2018). Although atmospheric deposition of Ba is small; accumulation in the snow and sea ice is a possibility; indeed, Hendry et al. (2018) suggested that dust might have supplied anomalously high Ba they observed in sea ice north of Svalbard. We note, however, that during the GN01 campaign, dBa in sea ice correlated with salinity (suggesting seawater intrusion) and snow samples did not indicate evidence of dust deposition great enough to result in substantial concentrations of dBa in sea ice (Marsay et al., 2018). Therefore, the sea ice endmember (dBa_{ice}) was estimated as the mean of sea-ice Ba concentrations collected during the GN01 expedition (Marsay et al., 2018). The minimum and maximum sea-ice estimates are set at plus or minus one standard deviation of the sea-ice samples.

3.2.2. Sensitivity Analyses

In general, analytical uncertainty is small relative to the range of plausible end-member compositions. Thus, we selected a couple variations of sensitivity analyses to determine the robustness of our results. We first examined a perturbation test where endmember values were varied by ±15%. We additionally examined the effect of using the plausible ranges of our endmembers (Table 1, Section 3.2.1). The results of these sensitivity analyses are described in further detail in the Supplemental (Text S7, Table S4 and Figures S5–S6 in Supporting Information S1). In general, for Ba_{pred} (Section 5.1), there is less than 10% uncertainty with respect to endmember selection. By propagating uncertainties of dBa_{pred} and dBa_{obs} we estimated that $Ba_{anomaly}$ has an uncertainty ~11% (generally around 5 nmol kg^{-1}). Ba isotope ($\delta^{138}Ba$) optimizations (Section 5.2) were insensitive to variations in endmember selection as described by the two methods above (15% variance or ranges). The optimizations were further insensitive to sea ice concentrations between 2 and 60 nmol L^{-1} (highest reported dBa in Arctic sea ice; Hendry et al., 2018). The box model (Section 5.4) was most sensitive to perturbations in the inventory and the residence time (a ~35% and ~30% change in the net nonconservative flux for a 15% perturbation, respectively). In terms of the expected endmember range, the model was most sensitive to changes in the Atlantic dBa endmember and volume fluxes. The model was insensitive to changes in the meteoric composition. The most plausible box model outcomes are presented in Section 5.4.

4. Results

4.1. Dissolved Ba Distribution

Dissolved Ba profiles in the Amerasian Basin were atypical of global ocean profiles. Contrary to the typical profiles of the Atlantic and Pacific where dBa is low in the surface and increases with depth (Chan et al., 1977), we observed high concentrations of dBa (>60 nmol kg^{-1}) in surface waters (0–~350 m; $\sigma_\theta < 27$ kg m^{-3}; Figures 2 and 3) in the Amerasian Basin, a decrease in dBa at intermediate depths (~350–2,000 m), and an increase in deep waters (>2,000 m). High concentrations between ~100 and 350 m depth are associated with a silicate maximum,

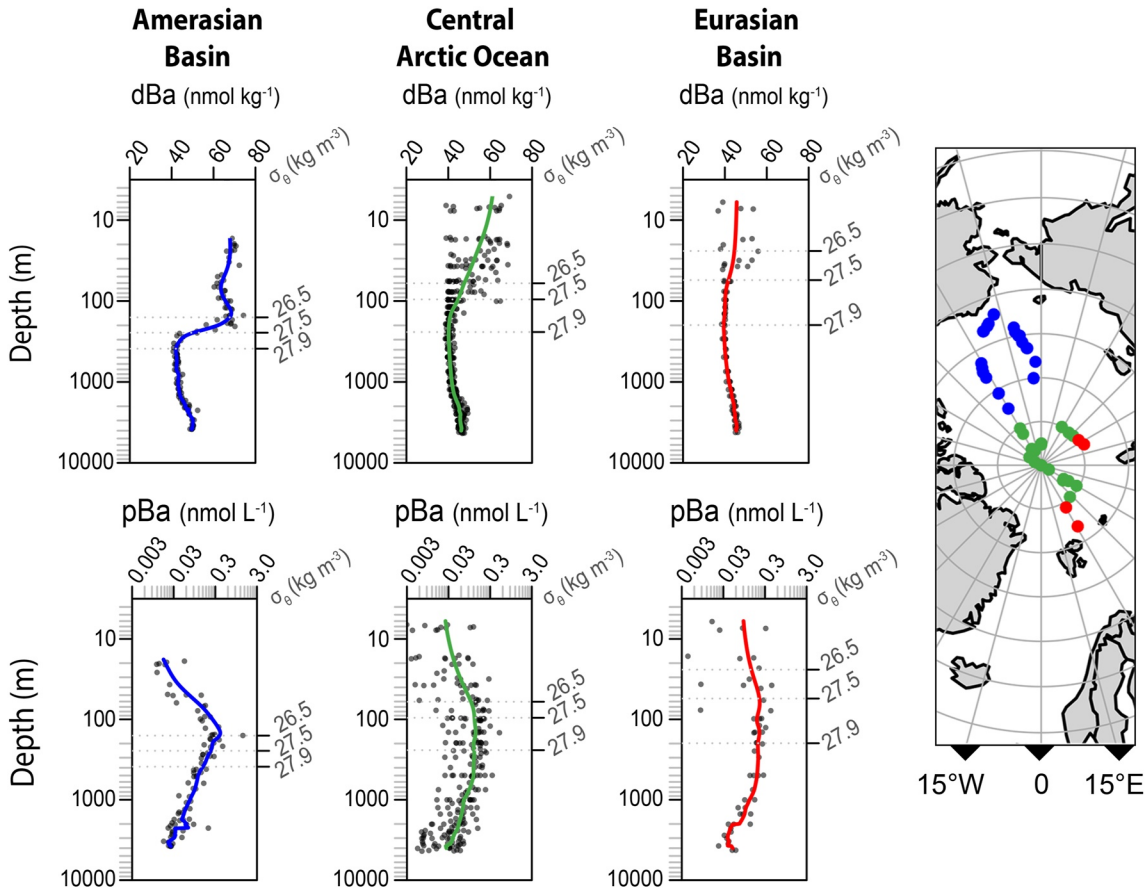

Figure 2. Mean profiles of dissolved and particulate Ba in the Amerasian, central, and Eurasian Arctic Ocean. Data used for mean profile come from the locations indicated in the map where the Amerasian Basin is blue, the central Arctic Ocean is green, and the Eurasian Basin is red. Approximate depth of relevant water masses are indicated by their corresponding potential density (σ_θ): 26.5 kg m^{-3} is Pacific Winter Water; 27.5 kg m^{-3} is the Atlantic Halocline; 27.9 kg m^{-3} is the Atlantic Layer. Notably, PWW is only observed in the Amerasian Basin, which is evidenced by the maxima in both dBa and pBa at that isopycnal.

which has been attributed to remineralization along the shelf (e.g., Jones & Anderson, 1986). Comparatively, dBa profiles in the Eurasian Arctic Ocean, Baffin Bay, and Lancaster Sound were similar to global ocean distributions. Additionally, deep water dBa concentrations in the Eurasian Arctic Ocean do not increase to concentrations as high as those observed in deep waters of the Atlantic or Pacific (Bates et al., 2017; Hsieh & Henderson, 2017; Schlitzer et al., 2018; see Figure S3 in Supporting Information S1).

Samples collected in the Chukchi and Bering Seas had a large range in dBa (11.9–84.5 nmol kg^{-1}; Figure 3). The extremes of this range are at one station (Station 2) influenced by a strong vertical gradient in dBa. Other shelf stations did not have as strong of a vertical gradient in dBa and were generally well mixed (Figure 4). Comparatively, the Barents Sea shelf had canonical profiles with low dBa (~32–40 nmol kg^{-1}) in the surface 100 m, increasing below that to roughly 42–43 nmol kg^{-1}. The CAA shelf (through the Parry Channel) was typified by concentrations between 50 and 65 nmol kg^{-1}.

Concentrations of dBa in the PML (defined at the depths where the change in density per meter is ≥0.1 kg m^{-4}) ranged between 39.0 and 69.3 nmol kg^{-1}, concentrations <53.1 nmol kg^{-1} were only observed in the Eurasian Arctic Ocean basins. Waters were slightly supersaturated with respect to barite (Ω_{barite} ~1.5) in the Amerasian Basin PML, but undersaturated in the Eurasian Arctic Ocean PML. Waters in the Baffin Bay and Labrador Sea mixed layer were also under- or near saturation with respect to barite, and waters in the Parry Channel were slightly over- or near saturation. PML waters are influenced by advection of Pacific-derived waters, riverine input, shelf modification, and sea ice formation or melt (Carmack et al., 2016; Kipp et al., 2018). The influence of sea ice melt on PML waters was evident in the marginal ice zone (GN01 Stations 8–19); surface dBa concentrations decreased where the fraction of sea ice melt increased (Pearson's $r = -0.9$ for stations 8–19 compared to

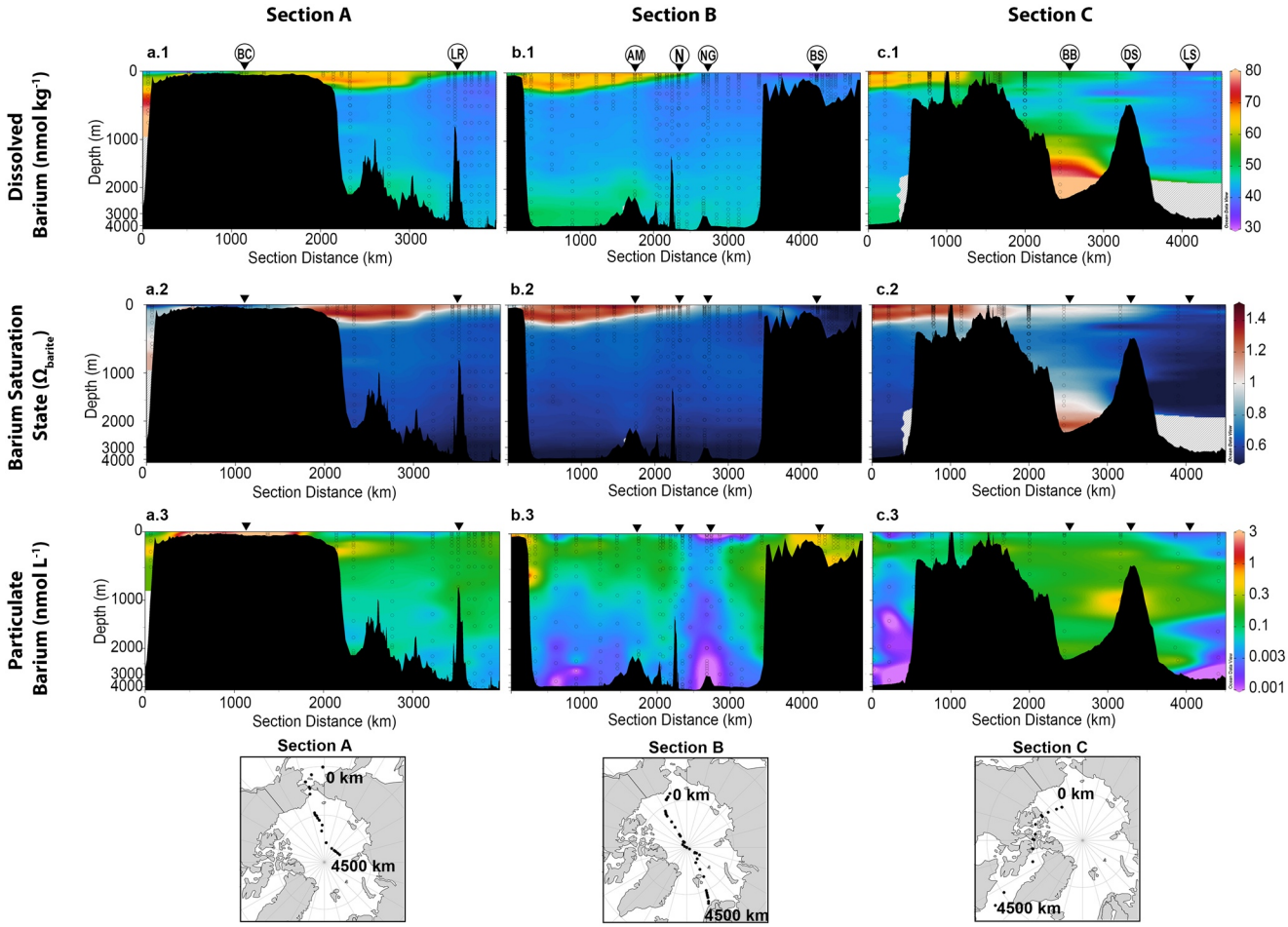

Figure 3. Distributions of dissolved and particulate Ba in nmol kg^{-1} and nmol L^{-1}, respectively. Each row of the figure represents a data type (i.e., same *z*-axis); each column represents a section (i.e., same *x*-axis). The rows across share the same *y*-axis and *z*-axis, viewed right of the panels. (a.1, b.1, and c.1) dBa; (a.2, b.2, and c.2) Barium Saturation State; (a.3, b.3, and c.3) total pBa for Sections A, B, and C, respectively, with a pBa depicted on a logarithmic scale. Hashed areas indicate the background where no data was available. Location of each section is indicated in the map below each section panel. Geographic features are noted by triangles above the section plot, the labels are at the top of the dBa Section. For Section A: AM = Alpha-Mendeleev Ridge, N = North Pole, NG = Nansen-Gakkel Ridge, BS = Barents Sea. For Section B: BC = Bering and Chukchi Seas (the marker is placed at the Bering Strait), LR = Lomonosov Ridge (the LR is also in Section A, west of the North Pole). For Section C: BB = Baffin Bay, DS = Davis Strait, LS = Labrador Sea.

$r = -0.4$ for Stations 8–65). Low concentrations of dBa were observed in sea ice sampled during this expedition (Marsay et al., 2018); thus, the melting of sea ice should dilute surface dBa.

The PH is comprised of PWW and PSW (discussed in Section 2.1). The highest dBa was observed in PWW (60.9–74.4 nmol kg^{-1} dBa; Figure 2) and slightly lower concentrations were observed in PSW (58–70.7 nmol kg^{-1} dBa; Figure 2). Dissolved Ba in both of these water masses was higher than the incoming Pacific water (56 ± 1 nmol kg^{-1}). Pacific Halocline waters were slightly above saturation with respect to barite ($\Omega_{barite} \sim 1.4$). Below the halocline waters, dBa decreased due to mixing with Atlantic-derived water. These intermediate waters were slightly undersaturated with respect to barite in both the Amerasian and Eurasian Basins.

In comparing the deep basins (>2,000 m), dBa was highest in Baffin Bay (>90 nmol kg^{-1}). Amerasian deep basins (i.e., Canada and Makarov basins; Figures 3a.1 and 3b.1) had average dBa of 47.9 ± 1.9 nmol kg^{-1} and the Eurasian Arctic Ocean (i.e., Amundsen and Nansen basins) deep water had average dBa equal to 45.5 ± 1.0 nmol kg^{-1}. Even though the Amerasian and Eurasian Basin deep water averages are not statistically different, dBa in the Amerasian deep basins ranged up to 52.5 nmol kg^{-1}, compared to dBa in the Eurasian basins, which ranged up to 47.3 nmol kg^{-1}. Thus, the Amerasian Basin deep waters had slightly higher dBa than the Eurasian Basin. Baffin

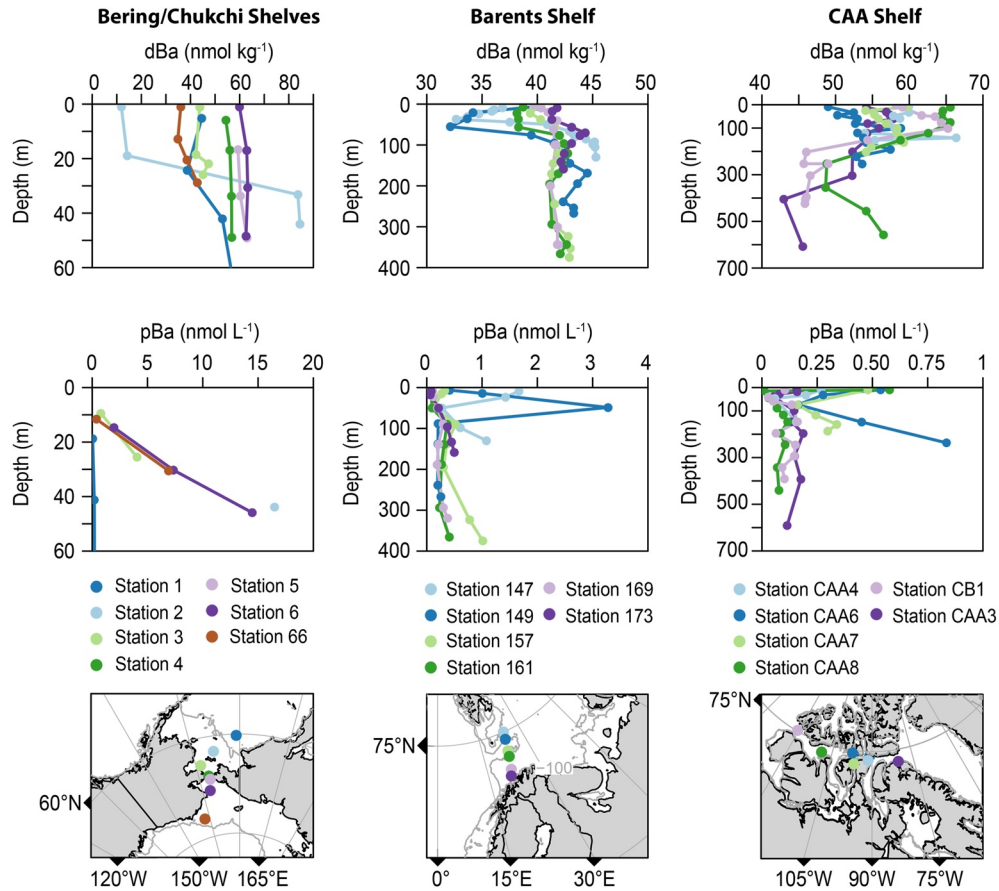

Figure 4. Shelf distribution of dBa and pBa. Left column depicts dBa and pBa profiles on the Bering and Chukchi shelves. Center column depicts dBa and pBa profiles on the Barents Sea shelf and the right column depicts dBa and pBa on the shelves of the CAA. Station 1 (Bering/Chukchi Seas) has data that exceeds the depth of the plot because it is on the Bering Sea Slope; it is included in these plots to represent the incoming shallow waters.

Bay deep waters were near saturation or slightly supersaturated ($1 < \Omega_{barite} < 1.5$), all other deep basin samples were undersaturated with respect to barite.

4.2. Particulate Ba Distribution

Arctic Ocean basins had pBa concentrations up to ~1 nmol L^{-1} (Figure 3). Maximum pBa concentrations were observed in the upper 500 m of the water column and were highest near the continental slope (Figure 3). Lithogenic contribution to the upper 500 m is consistently <10%. At stations where the PH is present (Amerasian Basin), the pBa maximum at each station was roughly at the core of PWW (0.17–1.37 nmol L^{-1} pBa; Figure 2). Comparatively, in other open ocean regions, the pBa maximum (roughly 200–1,000 m) is rarely >1 nmol L^{-1} and typically coincides with the top of the mesopelagic (Text S8, Figure S7 in Supporting Information S1; Bishop, 1988; Dehairs et al., 1997; Jacquet et al., 2005; Lam & Marchal, 2015). We attribute high pBa in PWW to lateral advection of shelf bottom waters into the basin. Comparatively, it appears that lateral advection of shelf waters into the Eurasian Basin from regional shelves is less particle rich.

Indeed, Bering and Chukchi Shelf concentrations of pBa were up to 16 nmol L^{-1}. Lithogenic particles in this region can support ~50% of the observed pBa. The highest pBa concentrations in this region are observed near the bottom (Figure 4). On the Barents Sea shelf, the maximum pBa concentration is 1.4 nmol L^{-1}, measured in a near-surface sample at ~20 m depth. Some regions of the Barents Sea shelf do show an increase in pBa near the bottom—up to ~1.0 nmol L^{-1} (Figure 4). Barents Sea pBa distributions thus indicate both active surface production of barite, likely associated with the oxidation of organic matter, and resuspension of the bottom sediments

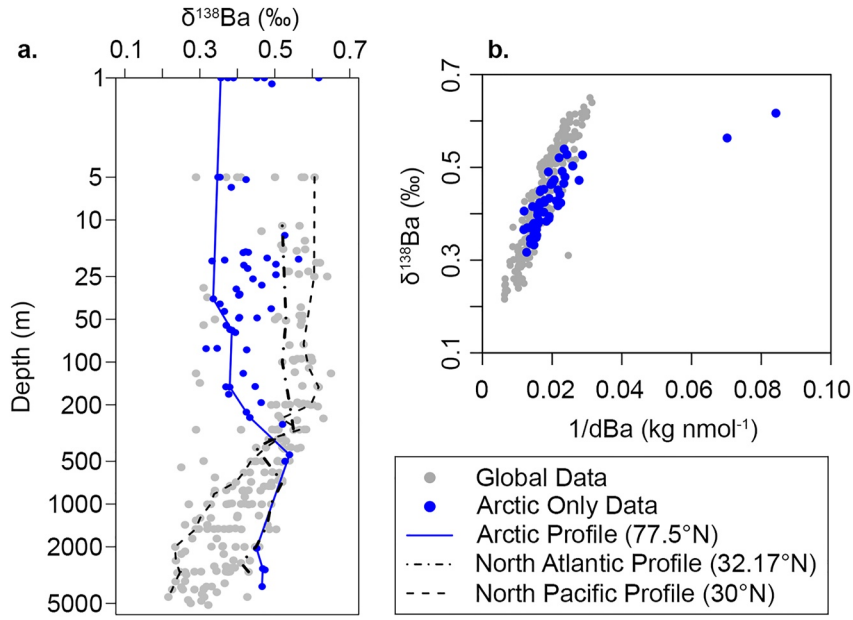

Figure 5. Arctic dissolved δ^{138}Ba distribution. (a) The vertical distribution of Arctic Ocean data (blue dots) and global data (gray dots). The depth axis is logarithmically scaled to expand the surface range. Solid blue and dashed and dotted black lines are example Arctic Ocean, North Atlantic Ocean, and North Pacific Ocean profiles, respectively. (b) The dissolved δ^{138}Ba vs. 1/dBa pattern.

as pBa sources. Indeed, the distribution of lithogenic and non-lithogenic pBa on the Barents Sea shelf supports this assessment; nearly 100% of the surface pBa (<100 m) is non-lithogenic while 100% of bottom water pBa (>200 m) are lithogenic.

During our sampling, pBa was <1 nmol L^{-1} in the CAA profiles (Figures 3 and 4). Profiles in the western CAA had low pBa throughout most of the water column, excepting some surface highs (Figure 4, see stations "CAA8" and "CB1"). Moving eastward a low pBa signal was carried through the CAA at a depth of ~75 m; profiles in the eastern CAA were characterized by a minimum at this depth (Figure 4). At stations east of "CAA8," pBa in surface waters was predominantly non-lithogenic, whereas below the subsurface minima pBa increased to 100% lithogenic composition.

4.3. Dissolved Ba Isotope Distribution

As with dBa, the shape of the δ^{138}Ba profile in the Amerasian Basin differed from observations made in other ocean basins: the surface was isotopically light and δ^{138}Ba increased to a maximum near 500 m. Below 500 m, δ^{138}Ba became lighter and the value stabilized below 2,000 m (Figure 5a). Interestingly, despite a different vertical profile shape, the local Arctic Ocean δ^{138}Ba versus 1/dBa relationship was generally similar to the global pattern (Figure 5b), which shows a positive correlation between δ^{138}Ba and 1/dBa.

The δ^{138}Ba value decreased across the Chukchi Shelf: the heaviest values were in the Bering Sea and δ^{138}Ba generally became lighter moving northward into the Chukchi Sea. The lightest values were in Chukchi Sea bottom waters and in PH depth waters (~50–150 m in the Amerasian Basin; Figure 6). Comparatively, dBa generally increased from the Bering Sea into the Chukchi Sea and the PH (Figure 4). Station 66, on the Chukchi Sea shelf, which is not depicted in Figure 6 section, did not follow this pattern and had both lower dBa and heavier δ^{138}Ba (Figures 4 and 6b). Station 2, on the Bering Sea shelf, also stands out as it had the lowest surface dBa concentrations and highest bottom dBa concentrations (Figure 4); δ^{138}Ba at this location was heavy in surface waters and light in bottom waters (Figure 6b). Interestingly, the surface waters at this station account for two samples that deviate from the global trend, which may imply these waters had undergone substantial particulate pBa formation in the surface.

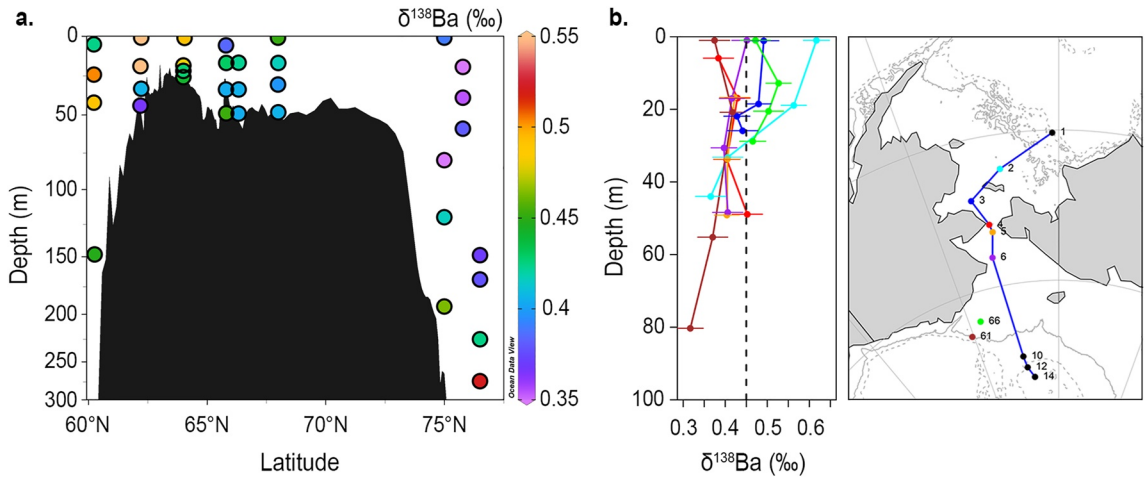

Figure 6. δ^{138}Ba distribution over the Bering and Chukchi Seas. (a) The shelf section depicting dissolved δ^{138}Ba on the *z*-axis; the map to the right identifies the section with a blue line. (b) Individual shelf station profiles, including two profiles from the Chukchi Sea that are not included in (a). The dashed line references surface waters in the Bering Sea (Station 1).

5. Discussion

High dBa surface waters in the Amerasian Basin were associated with the PML and the PH (Figure 2). Importantly, Atlantic-derived waters (~42 ± 3 nmol kg^{-1}) and incoming Pacific water (~54 ± 5 nmol kg^{-1}) both have lower concentrations than what we observed in the PH (Table 1), suggesting a significant endogenous Arctic source of dBa. In the following sections, we evaluate Ba sources and sinks and assess their influence on the dBa distribution. First, by investigating $Ba_{anomaly}$, we identify excess dBa in the PH waters of the Amerasian basin. Second, the δ^{138}Ba distribution indicates that processes over the shelves lightens the δ^{138}Ba signal, relative to incoming Bering Sea seawater (Section 5.2). Next, an Arctic Ocean basin box model reveals that conservative dBa sources and sinks account for 50%–80% of the dBa budget; implying non-conservative sources/processes contribute 20%–50% of the dBa budget (Section 5.3). We consider that non-conservative sources likely include sedimentary fluxes of authigenic or terrigenous dBa (Section 5.4). Further, we discuss the how the deep Arctic may acquire its dBa signal (Section 5.5) and the role of sources and sinks on the communication of Arctic Ocean geochemical properties to the North Atlantic (Section 5.6).

5.1. Assessing Observed dBa Distributions Relative to Predicted dBa

Our dBa distributions indicate a source of Ba to the water column that cannot be accounted for by the Pacific or Atlantic endmembers. Here, we investigate $Ba_{anomaly}$ (i.e., the difference between observed Ba and the Ba predicted from conservative mixing; Equations 3 and 4) to identify regions where mixing of water masses can and cannot explain the observed dBa distribution (Figure 7).

Significant negative anomalies (deficits) were observed in surface waters (<50 m) of the Transpolar Drift in Section B (Figure 7). Excesses (positive anomalies) were observed in the Amerasian Basin at depths associated with Pacific-derived seawater. The magnitude of particulate Ba abundance cannot account for the size of the anomalies (i.e., if particle cycling were a source/sink of dissolved Ba). Thus, the unequal magnitude of the surface deficit and excesses at Amerasian Basin stations implies that vertical redistribution from the shallow formation and deeper dissolution of Ba-bearing particles cannot strictly account for the observed $Ba_{anomaly}$ distribution.

Transpolar Drift waters—which originate from the East Siberian and Laptev Seas—most strongly influence the surface 50 m and have both a shelf and riverine component (Charette et al., 2020; Kipp et al., 2018). Charette et al. (2020) reported a significant trend between dBa and the fraction of meteoric waters within the TPD. While this trend roughly extrapolates to a riverine endmember compatible with Eurasian river dBa, they noted that scatter in the trend may be indicative of shelf processes such as cycling and redistribution of dBa and/or a shelf source of dBa (Charette et al., 2020; Kipp et al., 2018; Roeske, Bauch, Rutgers van der Loeff, & Rabe, 2012). The observed dBa deficit in these TPD waters (Figure 7) suggests that, at the time TPD waters were advected from the

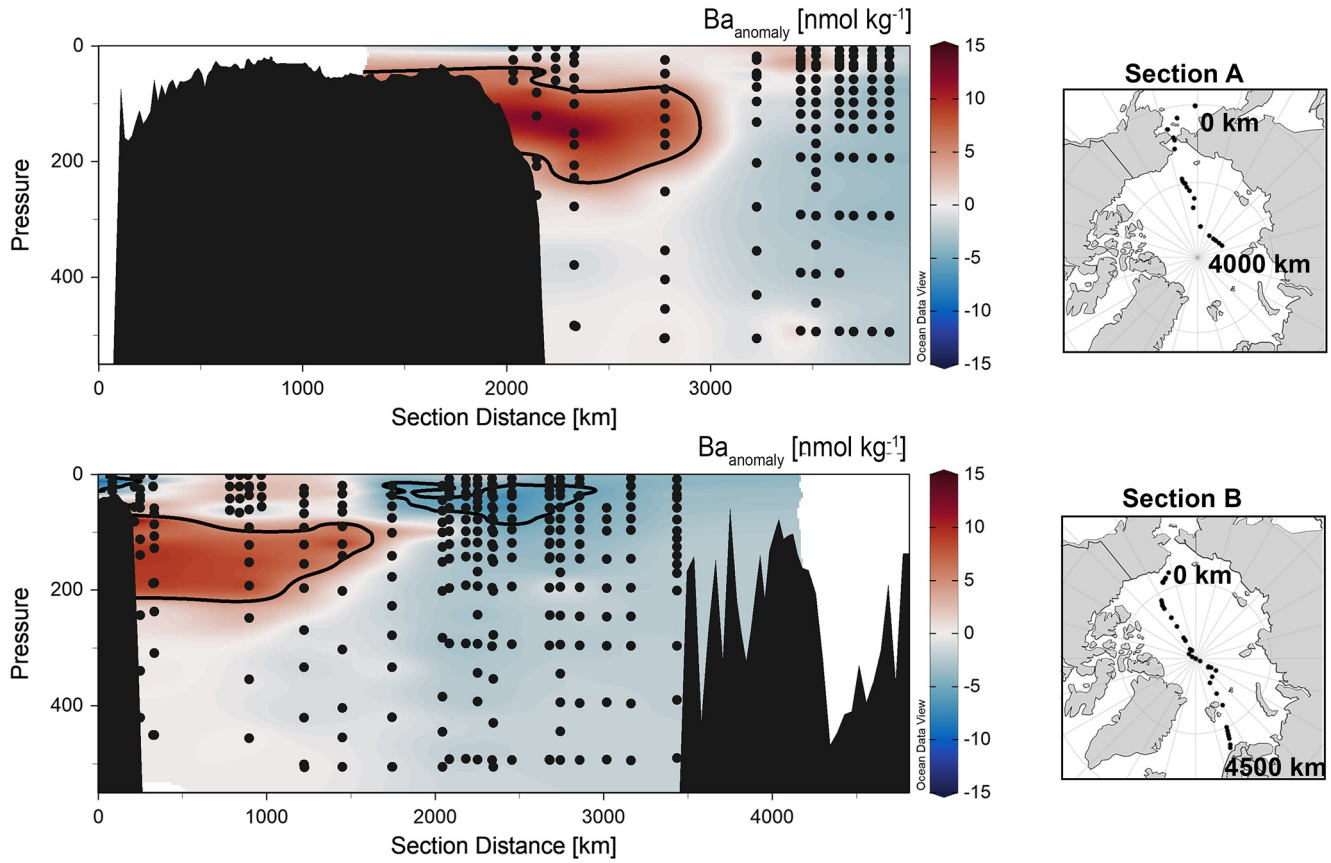

Figure 7. $Ba_{anomaly}$ (nmol kg^{-1}) for Sections A and B in the Arctic Ocean basins. $Ba_{anomaly} = 0$ (white tone) indicates the expected $Ba_{anomaly}$ for conservative behavior. Red tones indicate a source not considered in the Ba_{pred} model, and blue tones indicate a removal term. The solid black contours indicate where the $Ba_{anomaly}$ is significantly different from zero. Black points are where samples were collected.

shelves, the net effect of shelf processes on the dBa distribution in shelf surface waters was removal of dBa. This result agrees with observations in the Laptev Sea by Roeske, Bauch, Rutgers van der Loeff, and Rabe (2012), wherein dBa and f_{met} distributions were decoupled as a result of particle formation and export.

In comparing regions, the Amerasian Basin is influenced by a dBa source that is incorporated into Pacific-derived water while the Eurasian Basin does not appear to have an equivalent source. We attribute the basin-scale difference in $dBa_{anomaly}$ distributions to a greater amount of shelf-derived dBa from Amerasian shelves. However, the differences could also imply different margin sources (i.e., authigenic vs. terrigenous origin). The margin source of Ba is considered further in Section 5.4.

5.2. Ba Isotopes in the Upper Water Column: Implication of a Margin Source

The upper water column of the Arctic Ocean basins has large lateral advective fluxes that influence dissolved and particulate distributions (e.g., Aguilar-Islas et al., 2013; Rudels, 2018).

Given the application of dBa as a water mass tracer in the Arctic Ocean and the sensitivity of $\delta^{138}Ba$ to basin-scale mixing, it follows that the distribution $\delta^{138}Ba$ in the upper water column of the Arctic Ocean should also reflect conservative mixing of end-member Ba sources. However, similar to dBa, internal cycling and margin sources could influence the $\delta^{138}Ba$ distribution. Authigenic formation of pBa would leave the water column isotopically enriched in heavy Ba and lateral transport of shelf particulates should not influence the dissolved Ba isotopes. As mentioned in Section 4.2, $\Omega_{barite} \approx 1$ (implying saturation with respect to barite) in these waters; we expect little dissolution of barite particles in these waters and note that precipitation of Ba in the presence of organic matter nucleation sites is a possibility (Deng et al., 2019).

To test if the δ^{138}Ba distribution is supported by conservative mixing alone, we compared observed δ^{138}Ba with predicted δ^{138}Ba ($\delta^{138}Ba_{pred}$). The predicted δ^{138}Ba was determined by a linear mixing model (Equation 6). The denominator, dBa_{pred}, is defined in Equation 3; additionally, throughout Equation 6, δ^{138}Ba is identified as δ to improve readability.

$$\delta_{pred} = \frac{(\delta_{met} \times dBa_{met} \times f_{met}) + (\delta_{atl} \times dBa_{atl} \times f_{atl}) + (\delta_{pac} \times dBa_{pac} \times f_{pac}) + (\delta_{ice} \times dBa_{ice} \times f_{ice})}{dBa_{pred}}. \quad (6)$$

Endmember δ^{138}Ba values have not previously been determined for this region and endmember dBa is articulated in Section 3.2.1 (Table 1). We assessed the available literature to determine a range of reasonable endmember δ^{138}Ba for each component. Riverine δ^{138}Ba composition compiled from global observations range between ~0.2‰ and 0.46‰ (δ^{138}Ba; Cao et al., 2020; Charbonnier et al., 2018; Gou et al., 2020; Horner & Crockford, 2021). Recent work in the Arctic Ocean estimates Eurasian rivers have effective δ^{138}Ba endmembers that range between ~0.20 ± 0.06‰ and ~0.31 ± 0.04‰ and have an average of roughly 0.23 ± 0.04‰ (Bridgestock, Nathan, Hsieh, et al., 2021).

Similar to dBa, estuarine effects may alter the "effective" δ^{138}Ba value (Bridgestock, Nathan, Paver, et al., 2021). In five rivers, studies identified that desorption from particles potentially fractionates δ^{138}Ba resulting in an effective dissolved endmember that is lighter than the dissolved river endmember (Bridgestock, Nathan, Paver, et al., 2021; Cao et al., 2021).

The Pacific endmember, as a mean of previously published data from the surface 200 m of North Pacific stations, is 0.61 ± 0.02‰ ($n = 10$; Geyman et al., 2019; Hsieh & Henderson, 2017). Our study sampled the surface waters (<55 m) of a station at the Bering Sea Slope. Considering regional proximity, we suspect these waters may be more representative of the water entering the Arctic Ocean than the data from the northeast Pacific; at this station our data ranged from 0.42‰ to 0.50‰ ($n = 3$; mean = 0.47‰). For the Atlantic endmember we referenced previously published surface (<200 m) data in the North Atlantic, which indicated a mean δ^{138}Ba of 0.53 ± 0.03‰ ($n = 10$; Bates et al., 2017; Hsieh & Henderson, 2017).

We ran an optimization procedure in R ("optim"; R Core Team, 2018) where our cost was defined as the sum of the squared normalized residuals (SSNR; Equation 7). We performed a Nelder-Mead optimization, which iteratively and randomly tested possible endmembers, returning endmember values where the model-observation misfits were lowest (i.e., minimum of SSNR). In this analysis, we calculated $\delta^{138}Ba_{pred}$ by assuming that the isotopic contributions from ice were negligible since both f_{ice} in our samples and dBa_{ice} are low. Our optimized endmembers were determined as: $\delta^{138}Ba_{met} = 0.33‰$, $\delta^{138}Ba_{atl} = 0.57‰$, and $\delta^{138}Ba_{pac} = 0.36‰$. Compared to our a priori estimates of δ^{138}Ba endmember values, the cost (SSNR, Equation 7) was reduced from 61 (with $\delta^{138}Ba_{pac}$ set to 0.45‰) to 26 (SSNR = 0 is perfect model-data agreement), indicating our optimization procedure yields a substantially improved model-observation fit.

$$SSNR = \Sigma\left(\frac{x_i - x_i'}{\sigma_{x_i}}\right)^2. \quad (7)$$

Optimized dissolved δ^{138}Ba endmember values for both $\delta^{138}Ba_{atl}$ and $\delta^{138}Ba_{met}$ were insignificantly different than our a priori estimates. However, $\delta^{138}Ba_{pac}$ was ≅0.1‰ lighter. To cause $\delta^{138}Ba_{pac}$ to be ≅0.1‰ lighter than the incoming Pacific water there must be modification to one of our endmember terms (i.e., removal of isotopically heavy Ba) or an additional isotopically light source term. We consider it unlikely that authigenic particle cycling contributes to the low δ^{138}Ba of the Pacific endmember. That is, lateral transport of shelf-derived particles should not impact the δ^{138}Ba signal of the PH unless there was significant dissolution of particulates, which we consider unlikely given that PH waters are supersaturated with respect to barite. Likewise, in situ particle formation should leave residual seawater with heavier δ^{138}Ba since particles generally exhibit significantly lighter δ^{138}Ba than corresponding seawater (e.g., Horner et al., 2015; von Allmen et al., 2010). Thus, conservative mixing and internal cycling cannot explain the observed δ^{138}Ba distribution and a margin source is likely. Indeed, the persistence of lighter δ^{138}Ba in shelf bottom waters and Pacific halocline waters provides support for our earlier hypothesis that there is substantial margin contribution to basin dBa.

5.3. Analysis of the dBa Budget

Our analysis of the dBa distribution (including evidence from both the dissolved $Ba_{anomaly}$ and dissolved $\delta^{138}Ba$) suggests an additional dBa source to the Arctic Ocean as well as a potential sink in surface waters. In this section we quantify the advective fluxes of dBa to determine the net magnitude of the nonconservative components. Dissolved Ba in the Arctic Ocean has advective sources from rivers, sea-ice, Pacific-derived sea water, and Atlantic-derived sea water. Dissolved Ba sinks may include particle interactions and transport out of the system. At steady-state, sources balance sinks (Equation 8):

$$(F_{rivers} + F_{pacific} + F_{atlantic} + F_{ice} + F_{margin}) - (F_{particles} + F_{transport.out}) = 0. \quad (8)$$

where F represents the flux of dBa from sources (rivers, Pacific-derived waters, Atlantic-derived waters, ice, and margin contributions) and sinks (in situ particle formation and circulation out of the system). Following the approach of Kipp et al. (2018), we assess the fluxes of Ba from these sources and sinks in the surface 500 m of the water column (all fluxes have units of mol yr^{-1}). An issue with this approach is that it does not account for the spatial heterogeneity of the Arctic Ocean water column and treats all regions of the Arctic Ocean as homogeneous in terms of Ba distribution and residence time. Furthermore, the approach assumes steady-state and cannot identify non-steady state behavior, which is plausible given ongoing environmental change in the Arctic. Even with the acknowledgment of these assumptions and the uncertainty they introduce, within the single box, steady state framework we can derive a first order assessment of whether Ba fluxes into and out of the box are in balance. Our budget retains the same boundaries (Text S9 and Figure S8 in Supporting Information S1) as the model by Kipp et al. (2018), but it differs by determining the net nonconservative flux rather than the shelf-only flux. We consider the "net nonconservative" term to be the sum of F_{margin}, F_{ice}, and $-F_{particles}$ and it is calculated by subtracting known source fluxes from known sink fluxes (Equation 9).

$$F_{net-nonconservative} = F_{margin} + F_{ice} - F_{particles} = F_{rivers} + F_{pacific} + F_{atlantic} - F_{transport.out}. \quad (9)$$

Fluxes of Ba from rivers, Pacific seawater, and Atlantic seawater were solved using the following form:

$$F_{source} = [Ba]_{source} \times Q_{source}, \quad (10)$$

where F_{source} represents the flux of Ba from rivers, Pacific seawater, or Atlantic seawater in mol yr^{-1}. F_{source} is determined as the product of the endmember concentration of dBa in that source ($[Ba]_{source}$ as nmol m^{-3}) and the volume flux (Q) of that source into the surface 500 m (m^3 yr^{-1}). The dBa endmembers ($[Ba]_{source}$) for rivers, Pacific seawater, and Atlantic seawater are as described in Section 3.2.1.

We used volume fluxes derived from the literature that are largely summarized in Kipp et al. (2018). The annual Pacific volume flux, measured in the Bering Strait in 2011 (Woodgate et al., 2012), is $3.5 \pm 0.3 \times 10^{13}$ m^3 yr^{-1}; the minimum and maximum estimates from this term are defined by the *mean* ± 1 *SD*. The Atlantic flux, a more difficult term to quantify because of the multiple pathways by which it enters the Arctic Ocean and its diffuse flow, is estimated at $2.1 \pm 0.1 \times 10^{14}$ m^3 yr^{-1} (Beszczynska-Möller et al., 2012). This value is the average net flux into the Fram Strait, and thus it is not representative of the total volume entering the system. Atlantic waters entering the upper 500 m Arctic Ocean water column are a combination of Fram Strait and Barents Sea-derived waters. We follow Kipp et al. (2018) in the choice of our "best guess" Atlantic flux for consistency. However, we use only the net Fram Strait flux (±1 *SD*) as opposed to using the range of fluxes for the Fram Strait and Barents Sea branches in determining the minimum and maximum since the majority of Barents Sea Branch Waters are observed below 500 m in the Arctic Ocean (Beszczynska-Möller et al., 2012; Rudels, 2015). The river flux term was determined from Haine et al. (2015) using data collected between the years 2000 and 2010; Q_{rivers} equals $4.2 \pm 0.4 \times 10^{12}$ m^3 yr^{-1}.

The three flux terms that make up the net nonconservative term remain unconstrained: F_{margin}, $F_{particles}$, and F_{ice}. We consider F_{margin} to be the dominant term and note that $F_{particles}$ and F_{ice} are assumed to be negligible. First, $F_{particles}$ is a sink term that is the result of particle formation (and export) occurring within the box. Although we described evidence of Ba removal in surface waters (i.e., negative $Ba_{anomaly}$, Figure 7) in Section 5.1, we expect the largest negative Ba anomalies indicate biological removal signals from shelf waters (i.e., removal occurred outside of the box). Smaller signals, such as those observed in the Eurasian basin are not expected to quantitatively impact the overall budget. Furthermore, we note that particle formation and export from the surface 500 m

Table 2
Estimated Fluxes of dBa From Arctic Ocean Sources and Sinks (mol yr^{-1})

	Years	Minimum flux ($\times 10^9$)	Best estimate ($\times 10^9$)	Maximum flux ($\times 10^9$)	Percentage of total sinks ("best-estimate")
Sinks					
Transport out	2015	20	22	25	100
	1994	21	22	23	100
Sources					
Pacific advection	2015	1.8	2.0	2.2	9
	1994	1.1	1.3	1.5	6
Atlantic advection	2015	7.8	8.9	10	40
	1994	7.8	8.9	10	41
Rivers	2015	0.34	0.55	0.88	2
	1994	0.32	0.51	0.82	2
Net	2015	8.1	11	15	48
Nonconservative (F_{shelf}, $F_{ice.in}$, $F_{ice.out}$, $F_{particles}$)	1994	10	11	14	51
Shelf (Ba:^{228}Ra-derived)	2015	5.7	9.1	19	41
	1994	NA	NA	NA	NA

would be considered a Ba sink and would offset the relative influence of F_{margin}. Although we do not quantify $F_{particles}$ directly, a substantial positive imbalance in the system is still indicative of a margin source.

We consider sea ice to be a negligible component because our models for Ba_{pred} and $\delta^{138}Ba$ endmember prediction were insensitive over a range of sea ice concentrations (Section 3.2.2; Text S7 in Supporting Information S1). This is likely because both dBa and the relative amount of sea ice waters were low in most samples.

To compare the 2015 data to the 1994 Arctic Ocean Survey, which replicates many of the stations in both the GN01 and GN04 transects (Figure S8 in Supporting Information S1), we modified the flux terms (Equation 10) to be more representative of the 1990s. Haine et al. (2015) reported Q_{rivers} of $3.9 \pm 0.4 \times 10^{12}$ m^3 yr^{-1} between 1980 and 2000. Woodgate et al. (2012) reported annual Pacific fluxes through the Bering Strait of $2.2 \pm 0.3 \times 10^{13}$ m^3 yr^{-1}. Given the uncertainty in our original Atlantic flux term and the few estimates available specific to that decade, we apply the same fluxes as the 2015 mass balance. There is no evidence of major changes in the dBa endmember concentrations between the 1994 and 2015 cruises.

To determine the flux of Ba out of the system ($F_{transport.out}$) we determined an average dBa inventory for the upper 500 m of the Arctic Ocean basin by trapezoidally integrating dBa in the surface 500 m of each station where the bottom depth was >1,000 m (see Figure S4 in Supporting Information S1 for a reference to the 1,000 m isobath and the stations within it). Station inventories (mol m^{-2}) were averaged and then multiplied by the area of the Arctic Ocean (where the bottom depth is >1,000 m) to determine an Arctic-wide dBa inventory of $(221 \pm 25) \times 10^9$ mol Ba. The flux of Ba out of the system ($F_{transport.out}$) was calculated as the inventory divided by the residence time of waters in the surface 500 m. The residence time of waters in the surface 500 m is ~1–30 yr (Kipp et al., 2019; Schlosser et al., 1999), but in treating the surface 500 m homogeneously we selected a residence time of 10 yr. To determine the minimum and maximum shelf terms, we calculated the balance with the maximum source terms and minimum sink terms (minimum shelf input) and vice versa (maximum shelf input). We note, that while we applied a single residence time, decreasing the residence time results in a larger positive imbalance. Increasing the residence time to ≥20 yr can effectively resolve or produce a negative imbalance. Because the Ba supply and sink features (as identified by $Ba_{anomaly}$) are in waters with residence times <15 yr, we consider 10 yr to be a good approximation to investigate these features.

The results of the source-sink analysis reveal that around half (~52%) of the dBa transported out of the Arctic is accounted for through conservative mixing of dBa sources. This implies that net nonconservative sources are roughly 48% of the budget (Table 2). Since this approach effectively homogenizes the upper 500 m of the water column, redistribution within our box is neither a source nor sink; thus, our results indicate there must

be an external source to the box. This box model approach is sensitive to the endmember terms and fluxes (Section 3.2.2; Text S7 and Figure S6 in Supporting Information S1). Our model is most sensitive to the residence time of waters and the inventory, which set the fluxes of Ba out of the system ($F_{\text{transport.out}}$); it is further sensitive to endmember and flux of Atlantic waters. Increasing the flux of Atlantic Waters to the Barents Sea volume flux (rather than the Fram Strait volume flux) decreases the net nonconservative component to 20% of the budget. In actuality, the volume flux of Atlantic water in the surface 500 m box is some combination of water entering the Arctic Ocean through Fram Strait and Barents Sea, and not solely one or the other. Regardless, our estimate indicates there is a substantial net nonconservative source to the surface 500 m of the water column.

Since Ba can have large margin fluxes (e.g., Ho et al., 2019; Mayfield et al., 2021) we expect a substantial part of the net nonconservative flux term to be from the margins rather than local sea ice or particles. In the Arctic Ocean, flux from shelf sediments has been reported to account for up to 80% of the ^{228}Ra budget (Kipp et al., 2018). Although, unlike Ra, Ba fluxes from the margin are not contingent on radioactive decay, Ba also emanates from the sediment and, thus, Ra and Ba are often linearly correlated in seawater (the sources of Ba to the margins are discussed further in Section 5.4). We utilized this relationship to independently calculate F_{margin} by taking the product of the dissolved Ba to radium (dBa:d^{228}Ra) ratio over the Chukchi shelf (Text S10 and Figure S9 in Supporting Information S1) and the ^{228}Ra margin flux ($F_{\text{Ra.margin}}$, Equation 11). The dBa:d^{228}Ra ratio was determined from paired Ba and ^{228}Ra measurements during GN01 and $F_{\text{Ra.margin}}$ is from a box model estimate (Kipp et al., 2018). In doing so, we estimated F_{margin} accounting for 41% (range 23%–97%) of the inputs relative to sinks, which effectively closes the mass balance and is of equivalent magnitude to our box model analysis. This analysis operates under the assumption that the sources of both elements are similar. We also specify that the dBa:d^{228}Ra of GN01 Chukchi Sea samples may not well characterize all Arctic Ocean shelf systems, but this exercise affords us an additional constraint on margin Ba fluxes.

$$F_{margin} \simeq \frac{d\,Ba}{d^{228}\,Ra} \times F_{Ra.margin}. \tag{11}$$

Our flux balance approach indicates ~50% of the Ba budget must come from an additional source (i.e., F_{margin} F_{ice}, or $-F_{\text{particles}}$), which we hypothesized was likely the continental margins. Similarly, the Ba:^{228}Ra ratio, suggested ~40% of the Ba budget could be derived from the margins. Furthermore, the $\text{Ba}_{\text{anomaly}}$ and δ^{138}Ba distributions both indicate the need for an additional Ba source to the Arctic Ocean. Thus, while each of our approaches has uncertainties, they are all supportive of our hypothesis of a significant margin source of Ba in western Arctic Ocean.

For the 1994 Arctic Ocean Survey, we also found that the net nonconservative component of the budget was 51% (range: 45%–56%). Our data, within the uncertainties of the method, thus, do not reflect an increase in the net nonconservative flux of Ba between 1994 and 2015. However, we expected an increase in the margin Ba flux term following findings that the margin ^{228}Ra flux has increased between 2007 and 2015 (Kipp et al., 2018). Indeed, as Arctic Ocean shelves become more frequently ice-free, shelf chemical fluxes to the Arctic Ocean will increase (Charette et al., 2020; Kipp et al., 2018). While the apparent difference in temporal of change of Ba versus ^{228}Ra could be indicative of differing climate sensitivities of their sources, it may also simply result from the larger uncertainty of our Ba balance which is a consequence of the greater impact of Pacific and Atlantic advective sources of Ba relative to ^{228}Ra.

5.4. Supply of Shelf-Derived Ba to the Arctic Ocean Basins

Above, we have argued that the Arctic Ocean margins are a significant source of dBa, accounting for roughly half of the Ba budget in the upper 500 m of the Arctic Ocean. By investigating the distributions of dBa in the CAA (additional discussion in Section 5.6) and the Amerasian, central, and Eurasian Arctic Ocean it appears the largest dBa sources are from Amerasian margins (see Section 4.1). This contrast may relate to the shallowness of the Amerasian shelves as compared to the deeper Barents Sea and the regions of the CAA or to the relative nutrient supply and intensity of the local biological pump. To determine if our estimated dBa flux is reasonable, we divided the annual flux ($\sim 1 \times 10^{10}$ mol yr^{-1}) by the area of shelves in the Arctic (5.1×10^{12} m^2) and determined a shelf normalized dBa flux of 6 μmol m^{-2} day^{-1}. Although the mass balance assumes a well-mixed and evenly distributed source to the upper 500 m of the water column, the distribution of high dBa in the basins (e.g., Figure 7) indicates a more Amerasian source than Eurasian and higher concentrations over shallow Amerasian

Table 3
Estimated Area Fluxes of dBa From Arctic Ocean Shelves Compared With Studies From Other Shelf Systems

Region		Area weighted flux (μmol m^{-2} day^{-1})	Method	Publication
Arctic ocean	All shelf area	6	Box model	This Study
	All shelves except the Barents Sea	9		
	Chukchi, East Siberian, Laptev, and Kara Sea shelves	10		
California continental margin	—	<2	Benthic Chamber	McManus et al. (1998)
Tillamook bay estuary	—	2	Box Model	Colbert and McManus (2005)
Mississippi bight	—	35	Box Model	Ho et al. (2019)

shelves than the deeper Barents Sea in the Eurasian Arctic. We, thus, also estimated the flux with modified shelf area estimates. Using only the area of shallow broad shelves (~2.9×10^{12} m^2) including the Chukchi, East Siberian, Laptev, and Kara shelves; Jakobsson, 2002) dBa flux was 10 μmol m^{-2} day^{-1}; alternatively, using the total shelf area excluding the Barents Sea (~3.5×10^{12} m^2) dBa flux was 9 μmol m^{-2} day^{-1}. These results indicate a margin sedimentary flux of up to 10 μmol m^{-2} day^{-1} which is comparable to fluxes determined in other continental margin settings (Table 3).

Here, we review possible mechanisms supplying elevated dBa on the margins: (a) authigenic particulate Ba formation and dissolution in the water column or sediments and (b) continental sources of Ba.

First, we consider marine, authigenic, particle formation as a mechanism to redistribute dBa from shelf surface waters to shelf bottom waters. Authigenic pBa formation on the shelf may be associated with biological activity (e.g., Colbert & McManus, 2005; Hendry et al., 2018; McManus et al., 1994; Thomas et al., 2011), particle scavenging (Dymond et al., 1992), and brine-driven particulate barite formation (Hoppema et al., 2010). Considering observations from the Arctic Ocean's Laptev Sea, Roeske, Bauch, Rutgers van der Loeff, and Rabe (2012) hypothesized that vertical redistribution of dBa on the shelves, through particle formation at the surface and dissolution in the bottom waters, and subsequent advection to the basins supported the basin $Ba_{anomaly}$ profiles. For water column vertical redistribution to support our dBa and δ^{138}Ba distribution in the basin, a substantial spatial or temporal decoupling between surface and bottom shelf waters would be required. Since our mass balance is integrated over the upper 500 m of the water column, which includes laterally advected surface and bottom shelf waters, the water column remineralization would have to be decoupled at length scales greater than the residence time of the PML (~3 yr). Therefore, in conjunction with the $Ba_{anomaly}$ discussion (Section 5.1), dBa cannot simply be moved from the surface to the bottom shelf waters and a distinct sedimentary component must be considered.

Arctic Ocean margin sediments often have high biogenic Ba content, especially in association with the ice edge (Nurnberg, 1996). Evidence of sedimentary remineralization and diagenesis has been observed in the shallow Arctic shelves and in the PWW (e.g., Granger et al., 2018; Jones & Anderson, 1986). Sedimentary processes decoupled from water column processes could explain the signals of dBa, pBa, and δ^{138}Ba in the PH. Sedimentary Ba is isotopically light relative to the water column, with authigenic δ^{138}Ba of ~0.1‰ and detrital Ba ranging between~−0.1‰ and 0.0‰ (Bridgestock et al., 2018; Crockford et al., 2019). We thus suggest that authigenic pBa formation and remineralization in the water column does not wholly account for the shelf source, but sedimentary remineralization in addition to continental sources may.

Continental sources often have high dBa and low δ^{138}Ba (Gaillardet et al., 2014; Gou et al., 2020; Mayfield et al., 2021). Delivery of continental dBa to the marine system could be through river discharge, submarine groundwater discharge, and terrigenous particles. Through our previous sections (Section 5.1 and 5.3) we demonstrated rivers alone cannot support high dBa concentrations. Submarine groundwater discharge (SGD) has high dBa fluxes (e.g., Ho et al., 2019; Shaw et al., 1998) and light δ^{138}Ba (Mayfield et al., 2021); however, few studies have examined SGD fluxes in the Arctic shelf system. Although the overall impact and biogeochemical implications (especially for Ba) are presently unknown, site studies in the coastal region of northern Alaska and in the Laptev Sea describe highly variable SGD fluxes (Charkin et al., 2017; Lecher, 2017; Lecher et al., 2016). It is

also likely that, as permafrost thaws, SGD fluxes will increase (Lecher, 2017 and references therein) and, thus, the SGD component may become even more important to quantify. We consider that terrigenous sources, such as SGD or terrigenous particles, could contribute to the observed increase in dBa and decrease in the dBa isotopic composition in Amerasian Basin halocline waters. Broadly, the higher potential Ba contribution from the North American continent (relative to the Eurasian continent) combined with potentially large authigenic sedimentary sources of pBa in the Bering and Chukchi Seas and the large $Ba_{anomalies}$ in the Amerasian sector of the Arctic Ocean indicate that the source is coming from the North American shelves (Bering and Chukchi), although the shallow East Siberian Sea cannot be excluded as a possible source. From the isotopes, it is clear that there is a source of light dBa, relative to incoming Pacific waters. Both SGD and sedimentary remineralization of authigenic particles are lighter than the incoming pacific waters; we suggest that additional observations (especially ones that capture the annual shelf cycle and add spatial resolution to our shelf observations) are necessary to be able to quantify relative inputs from different sedimentary components.

Different Arctic Ocean shelf regions are likely to have unique responses to changing climatological regimes: the depth of the shelves (and amount of local resuspension), the relative nutrient supply, and the strength of the biological pump must be considered. Furthermore, the nature and quantification of the benthic contribution to the margin flux also needs to be further constrained. This, too, could be a factor contributing to our observation of different relative shelf fluxes between the Amerasian and Eurasian Basins and may be climate responsive: to what degree are the margin Ba sources of authigenic or terrigenous origin in different margin settings? We note that, like studies for other tracers (e.g., Charette et al., 2020; Kipp et al., 2018; Kipp, Henderson, Wang, & Charette, 2020), the Ba cycle in the Arctic Ocean may undergo changes in response to climate-driven sea ice retreat that increase relative influence of the non-conservative components (e.g., increased sedimentary resuspension from wind-driven turbulence/convective mixing, elongated growing seasons, and enhanced particle cycling).

5.5. Arctic Ocean Deep Water Ba

The trace element geochemistry of the deep Arctic Ocean basins has been little explored. It has been hypothesized that benthic fluxes and particle supply, hydrothermal supply, shelf-derived brine contributions, and age of the deep waters each influence the differences between the basins (e.g., Bauch et al., 1995; Kipp et al., 2019; Middag et al., 2011). Amerasian Basin deep waters had higher dBa (up to 53 nmol kg^{-1}) than Eurasian Basin deep waters (up to 47 nmol kg^{-1}). Baffin Bay deep waters had the highest deep dBa concentrations (>90 nmol kg^{-1}). In this section, we assess the likelihood of various proposed drivers of deep basin dBa distributions in the Amerasian Basin, the Eurasian Basin, and Baffin Bay. We note, within the framework of this study we cannot quantify relative inputs but instead we articulate where we see evidence of each source.

Hydrothermal sources are present in the Eurasian Arctic Ocean along the Nansen-Gakkel Ridge, an ultra-slow spreading center (Edmonds et al., 2003); this spreading center has been a source of trace elements in waters deeper than 1,000 m (Edmonds et al., 2003; Klunder et al., 2012). In this study, a peak of Ba between 2,000 and 3,000 m is evident at the station nearest the Nansen-Gakkel ridge crest (Text S11 and Figure S10 in Supporting Information S1); this feature matches, by depth range, dFe and dMn peaks observed in previous studies (Edmonds et al., 2003; Klunder et al., 2012; Middag et al., 2011). Although we identify that dBa flux is occurring from the ridge crest, the small (2–3 nmol kg^{-1}) signal and limited extent (i.e., observed at only one station) of the signal suggests this is a minor component of the deep Arctic Ba mass balance. Nonetheless, given that recent evidence that net hydrothermal $\delta^{138}Ba$ is heavy (Hsieh et al., 2021), analysis of $\delta^{138}Ba$ in the deep Eurasian Basin could be instructive regarding the importance of the Ba hydrothermal flux.

Diffusion from sediment pore waters is another potential source of dBa. Recent work suggests a diffusive benthic source of tracers to Baffin Bay Deep waters (Manning et al., 2020); this idea is supported by the vertical gradient in dBa (i.e., increasing toward the sediments). Importantly, diffusion from sediment pore waters is likely not distinct from dissolution of particles.

Dissolution of particles may also increase deep basin dBa. Deep waters in all Arctic Ocean basins were undersaturated with respect to barite (Figure 2) and thus, particle dissolution could drive increases in dBa. Ba particles to the Arctic deep basins may be from local surface production and vertical settling, advected shelf particles (by local currents or eddies) and subsequent vertical settling, injection pumps (such as sinking of brines), subduction

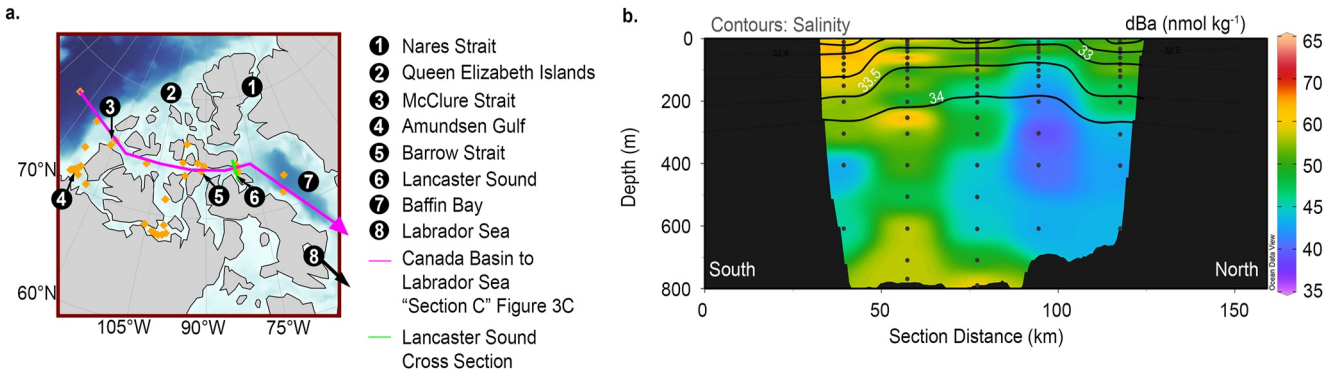

Figure 8. Dissolved Ba distributions in the Canadian Arctic Archipelago. (a) Geography of the CAA with pertinent features numbered and labeled. Sections investigated in this study are identified by purple and green lines. The purple line moves from the Canada Basin, through the Parry Channel, into Baffin Bay. (b) A cross-section of the Lancaster Sound depicting dBa on the z-axis; this cross section includes salinity contours from 32 to 34.5 at intervals of 0.5 (dBa data published in Mears et al., 2020).

of waters, or nepheloid layers or sea ice (Bauch et al., 1995; Boyd et al., 2019; Colombo et al., 2020; Hunkins et al., 1969; Hwang et al., 2015; Marsay et al., 2018; Roeske, Bauch, Rutgers van der Loeff, & Rabe, 2012; Roeske, Rutgers van der Loeff, Middag, & Bakker, 2012; Xiang & Lam, 2020). We considered the feasibility of particle dissolution as a source to the deep dBa by investigating the δ^{138}Ba decrease below 2,000 m in the Amerasian Basin (Figure 6). Here we calculated the δ^{138}Ba from an additional source (such as dissolving particles) required to decrease the isotopic signature using a simple two component mixing model such that:

$$\delta^{138}Ba_{source} = \frac{\left(\delta^{138}Ba_{obs} \times dBa_{obs}\right) - \left(\delta^{138}Ba_{initial} \times dBa_{initial}\right)}{dBa_{obs} - dBa_{initial}}. \quad (12)$$

The $\delta^{138}Ba_{source}$ was determined to be ~0.06‰ if deep Amerasian Basin waters ($\delta^{138}Ba_{obs}$ = 0.46 ± 0.01‰; dBa_{obs} = 52.5 nmol kg^{-1}) were strictly Atlantic in origin ($dBa_{initial}$ = 42 nmol kg^{-1} and $\delta^{138}Ba_{initial}$ = 0.55‰). In this scenario, the observed composition is the result of mixing the initial Atlantic-derived seawater with a single source (which realistically may be the net composition of multiple sources). This calculation assumes no mechanism for the additional source (or net isotopes of several sources); however, a $\delta^{138}Ba_{source}$ of ~0.06‰ is consistent with pelagic barite derived from surface waters possessing a δ^{138}Ba ≈ 0.5, assuming a Ba isotope fractionation during barite precipitation of roughly −0.5‰ (Horner et al., 2021).

Thus, we conclude that (in the Amerasian Basin), isotopic analysis is consistent with dissolution of vertically settling or injection of upper water column particles as a principal source of the deep basin dBa signature. In the Eurasian Arctic Ocean, the combination of particle dissolution (e.g., Bauch et al., 1995; Boyd et al., 2019) and hydrothermal supply likely influences deep basin dBa distributions.

Lastly in Baffin Bay, elevated dBa and pBa signals may be indicative of a nepheloid layer (Figure 3). Furthermore, an active seasonal biological pump could be important in Baffin Bay (Honjo et al., 2010; Lalande et al., 2009; Lehmann et al., 2019; Nöthig et al., 2020). Lemaitre et al.'s (2018) observation of high pBa in the deep Labrador Sea which was thought to be the result of bloom cycles and convective downwelling; a similar mechanism may be at play in northern Baffin Bay as well.

5.6. Ba in the Canadian Arctic Archipelago

The Canadian Arctic Archipelago (CAA) and Fram Strait are the two main pathways by which water exits the Arctic Ocean (Rudels, 2018) and they contribute roughly equivalent volume fluxes to the total outflow (Beszczynska-Möller et al., 2011). Our discussion above suggests the potential for the CAA transit to influence the outgoing Ba distribution, particularly by introduction of river waters and sediment-water column exchange. To consider this influence on dBa, we focus on the Parry Channel Section, which is the channel running between McLure Strait (Figure 8a, #3) and Lancaster Sound (Figure 8a, #6). This channel is a conduit for Amerasian Basin waters

leaving the Arctic domain through Baffin Bay (e.g., Colombo, Brown, et al., 2019). Generally, the distributions we observed in the Parry Channel and Lancaster Sound agree with previous observations described by Thomas et al. (2011) and Mears et al. (2020).

In the Parry Channel, the dBa distribution shows the influence of the PH west of Barrow Strait (Figure 3c1). These waters are typified by high dBa concentrations (~65 nmol kg^{-1}) at densities associated with the PH. Near the Barrow Strait, isopycnals associated with the PH ($\sigma_\theta \sim 27.5$ kg m^{-3}) shoal and dBa decreases by roughly 10 nmol kg^{-1}. This decrease could be driven by a few mechanisms: (a) sea ice melt, (b) dilution by local rivers, (c) particle formation in surface waters, or (d) dilution with low Ba seawater. Although rivers in the CAA have dBa between ~10 and 300 nmol L^{-1} (Colombo, Rogalla, et al., 2019), the decrease in dBa across Barrow Strait occurs at salinities between 32 and 33 and is not correlated with decreasing salinity, which excludes sea ice melt or river discharge as drivers of the dBa decrease (Text S12 and Figure S11 in Supporting Information S1). Oxygen isotopes of water ($\delta^{18}O$) are a good indicator of freshwater input but were not available for station on both sides of the Barrow Strait for this cruise (Thomas et al., 2021), and thus were not utilized in this analysis.

We suspect the dBa decrease eastward in the CAA is driven, in part, by mixing with "Baffin Bay-derived" waters. Specifically, in the Lancaster Sound cross section (Figure 8b) the Ba distribution reveals the influence of at least two water types: high dBa (~55 nmol kg^{-1}; $S < 33.5$) and low dBa (~45 nmol kg^{-1}; $S > 33.5$; Figure 8b). Surface dBa at all Lancaster Sound stations is roughly 55 nmol kg^{-1}. Below the surface layer, the dBa on the northern side of the Sound decreases to ~45 nmol kg^{-1}, while the stations on the south side tend to remain around 55 nmol kg^{-1}. These observations are consistent with the local circulation wherein Baffin Bay-derived waters flow westward on the northern side of the Sound and CAA-derived waters flow eastward on the southern side of the Sound (Prinsenberg et al., 2009). Thus, Baffin Bay-derived waters have the potential to erode the PH signal near Barrow Strait since they contain lower dBa. Thomas et al. (2011) and Mears et al. (2020) described the same dilution effect in the eastern CAA and also attributed it to Atlantic-origin waters in Baffin Bay entering Parry Channel. Furthermore, the same effect has been described for other tracers (Colombo, Brown, et al., 2019; Mears et al., 2020; Rudels, 1986; Top et al., 1980).

Particulate Ba patterns imply that a combination of surface productivity (oxidation of organic matter supporting non-lithogenic barite production), water mass mixing (driving pBa low in the subsurface), and sediment resuspension (as a source of lithogenic pBa in bottom waters) set the distribution. However, with the low pBa concentrations we observed, it is likely that the scale of the pBa cycle does not substantially influence the dBa distribution on relevant timescales in this section. Thus, mixing of water masses remains the likely driver of the dBa distribution.

Flux of dBa across Lancaster Sound, as the product of the Lancaster Sound cross-sectional mean (± 1 *SD*) and the range of net volume fluxes through Lancaster Sound into Baffin Bay (0.7 ± 0.3 Sv from Prinsenberg et al., 2009) is $1.1 \pm 0.6 \times 10^9$ mol yr^{-1}. This is slightly less than, though on the same order of magnitude as other estimates of dBa outflow through Lancaster Sound (Thomas et al., 2011; 1.6×10^9 mol yr^{-1}) and through the CAA (Taylor et al., 2003; $2.8 \pm 0.2 \times 10^9$ mol yr^{-1}).

The section through Baffin Bay (Figure 3c1) depicts high (~55 nmol kg^{-1}) dBa in surface waters to Davis Strait. Below ~100 m ($\sigma_\theta \sim 27$ kg m^{-3}) concentrations decline to 40–45 nmol kg^{-1}. In Baffin Bay, dBa increases again below the depth of the CAA and Davis Strait sills (~1,000 m), yielding dBa concentrations that are higher than observed in any other Arctic region, reaching ~105 nmol kg^{-1} (see Section 5.5 for further discussion). South of Baffin Bay, in the Labrador Sea, surface dBa concentrations are low (much more "Atlantic-like," ~42 nmol kg^{-1}) and influence from Baffin Bay high dBa values is not evident (Figure 2c). This suggests that there is drawdown of the surface dBa by dilution or internal cycling or that the locations sampled did not capture the outflow of Davis Strait.

Compared to our observations on the Bering and Chukchi Seas, and in the PH of the Amerasian Basin, the CAA shows minimal evidence of riverine influence or sedimentary sources on the dBa distribution. This result is unexpected; while one could invoke short residence times of water mass transit (~2 yr in the CAA for near surface waters, increasing residence time with deeper water masses; Rudels, 1986), the transit across the CAA is longer than that of waters of the Chukchi Shelf (6–8 months; Spall, 2007), and comparable to that of the East Siberian Arctic Seas (~6 months–3.5 yr (Bauch et al., 2009; Schlosser et al., 1995). Thus, we suggest that the time waters

spend on the shelf is not the main control on the level of shelf influence in the region. Instead, we suspect that water column depth is of primary importance in regulating the amount of sediment-water column exchange as wind-driven turbulence may support higher levels of sedimentary exchange in shallow environments. Indeed, although geography and geology in the CAA is highly variable (Colombo, Brown, et al., 2019), the CAA stations we investigated in this study have bottom depths >130 m (sill depth of Barrow Strait; Melling, 2000).

6. Conclusions

We conclude, through observations from four synoptic GEOTRACES expeditions, that Ba is not conservative in the Arctic Ocean. Previous studies have noted that nonconservative behavior of dBa in the Arctic Ocean may complicate its use as a tracer of river water sources (Hendry et al., 2018; Roeske, Bauch, Rutgers van der Loeff, & Rabe, 2012). Our pan-Arctic analysis, including dissolved and particulate data as well as isotopic composition, indicates that there is a substantial (~50%) Ba source term from the margin that cannot be accounted for solely by redistribution of dBa in the surface 500 m of the water column. We hypothesize that the endogenous Ba source originates from a benthic source along the Amerasian Margin with a flux magnitude between 6 and 10 μmol Ba m^{-2} day^{-1}. We suggest the application of dBa as a tracer only when one can verify that inputs from the margins are small or can appropriately make corrections to account for influence of the margins. Future work may look into the feasibility of utilizing dBa as a tracer in the basin PML, rather than the entire halocline; such work would need to consider the removal of Ba from PML source waters through pBa formation on the shelves. Alternatively, dBa and its isotopes may be suitable as a tracer of shelf sedimentary sources.

Over the long residence times of deep water in the basins, particle supply and dissolution may be a dBa source. In the Amerasian Basin, the composition of Ba isotopes in deep water are lighter than Atlantic derived seawater. The lighter isotopic signature is compatible with dissolution of particles formed in surface waters over the Chukchi Shelf. This conclusion is consistent with previous literature (Roeske, Rutgers van der Loeff, Middag, & Bakker, 2012) which used ratios of Ba:Si and Ba:Al to determine there was likely a substantial component of shelf material supplying the deep basin geochemical signatures. Through this study we cannot constrain the deep basin source of Ba strictly to particulate supply and dissolution; however, the available observations support that hypothesis.

The large margin Ba source reinforces the importance of contributions from the margins to basin geochemical distributions in the Arctic Ocean specifically (Charette et al., 2020; Jensen et al., 2019; Kadko et al., 2019; Kipp et al., 2018; Kondo et al., 2016; Marsay et al., 2018; Whitmore et al., 2019; Xiang & Lam, 2020), and perhaps more generally to the open oceans. Furthermore, it affirms the need to identify and quantify margin inputs at regional scales (e.g., Charette et al., 2016; Jeandel et al., 2011). This is evident from the large nonconservative Amerasian Basin dBa signal in the surface 500 m relative to Eurasian Basin. Additionally, the CAA dBa distribution is controlled by physical mixing of sea waters and we saw no evidence for a large benthic signal.

We suggest that further investigation into the sedimentary and particulate components of the Ba cycle is necessary. Comprehensive determination of Ba concentrations, isotopes, and fluxes from sediments as well as settling particle fluxes and composition will improve our understanding of the Arctic Ocean Ba cycle and allow us to better constrain the geochemical mass balance. Both measurements of in situ Ba concentrations and isotope composition as well as the composition of potential source materials (e.g., terrigenous particles, marine particles, submarine groundwater discharge, and fluvial and estuarine waters) are imperative to these efforts. Such constraints may allow us to better predict the way changing climate will impact dBa distributions and their applications in the Arctic Ocean. Furthermore, we acknowledge there is still great uncertainty into how Arctic Ocean deep basins obtain and maintain their geochemical signatures. In both the upper water column and deep basins, combined tracer approaches are an important direction to resolving the relative sources and sinks to each basin.

Data Availability Statement

Data used in this study are available at the Biological and Chemical Oceanography Data Management Office (DOIs: 10.26008/1912/bco-dmo.772645.2, 10.26008/1912/bco-dmo.807340.1), the EarthChem Library (DOI: 10.1594/IEDA/100,633), and PANGAEA (DOI: https://doi.org/10.1594/PANGAEA.896022).

Acknowledgments
This research was supported by the National Science Foundation [OCE-1434312 (AMS), OCE-1436666 (RN), OCE-1535854 (PL), OCE-1736949, OCE-2023456 (TJH), and OCE-1829563 (R. Anderson for open access support)], Natural Sciences and Engineering Research Council of Canada (NSERC)-Climate Change and Atmospheric Research (CCAR) Program (MTM), and LEFE-CYBER EXPATE (HP). HT acknowledges support by the Canadian GEOTRACES via NSERC-CCAR and the German Academic Exchange Service (DAAD): MOPGA-GRI (Make Our Planet Great Again—Research Initiative) sponsored by BMBF (Federal German Ministry of Education and Research; Grant No. 57429828). We thank the laboratory technicians that helped produce the data presented in this study: Melissa Gilbert (USM), Jacques Navez (VUB), Martine Leermakers (VUB), and Mette Kaufman (UAF). Christopher Guay contributed dissolved barium data from the 1994 Arctic Ocean Survey. Thank you to the scientific and operational crews of the USCGC Healy (GN01), the CCGS Amundsen (GN02 and GN03), and the R/V Polarstern (GN04). We have great appreciation for the support of the scientific PIs of the four cruises: Greg Cutter (GN01), Roger Francois (GN02 and GN03), Dave Kadko (GN01), Bill Landing (GN01), Kristin Orians (GN03), Michiel Rutgers van der Loeff (GN04), Ursula Schauer (GN04), and Phillipe Tortell (GN02).

References

Abrahamsen, E. P., Meredith, M. P., Falkner, K. K., Torres-Valdes, S., Leng, M. J., Alkire, M. B., et al. (2009). Tracer-derived freshwater composition of the Siberian continental shelf and slope following the extreme Arctic summer of 2007: Siberian freshwater. *Geophysical Research Letters*, *36*(7), L07602. https://doi.org/10.1029/2009GL037341

Aguilar-Islas, A. M., Rember, R., Nishino, S., Kikuchi, T., & Itoh, M. (2013). Partitioning and lateral transport of iron to the Canada Basin. *Polar Science*, *7*(2), 82–99. https://doi.org/10.1016/j.polar.2012.11.001

Alkire, M. B., Jacobson, A. D., Lehn, G. O., Macdonald, R. W., & Rossi, M. W. (2017). On the geochemical heterogeneity of rivers draining into the straits and channels of the Canadian Arctic Archipelago: Canadian Arctic rivers. *Journal of Geophysical Research: Biogeosciences*, *122*(10), 2527–2547. https://doi.org/10.1002/2016JG003723

Alkire, M. B., Morison, J., & Andersen, R. (2015). Variability in the meteoric water, sea-ice melt, and Pacific water contributions to the central Arctic Ocean, 2000–2014. *Journal of Geophysical Research: Oceans*, *120*(3), 1573–1598. https://doi.org/10.1002/2014JC010023

Andersson, P. S., Porcelli, D., Frank, M., Björk, G., Dahlqvist, R., & Gustafsson, Ö. (2008). Neodymium isotopes in seawater from the Barents Sea and Fram Strait Arctic–Atlantic gateways. *Geochimica et Cosmochimica Acta*, *72*(12), 2854–2867. https://doi.org/10.1016/j.gca.2008.04.008

Bates, S. L., Hendry, K. R., Pryer, H. V., Kinsley, C. W., Pyle, K. M., Woodward, E. M. S., & Horner, T. J. (2017). Barium isotopes reveal role of ocean circulation on barium cycling in the Atlantic. *Geochimica et Cosmochimica Acta*, *204*, 286–299. https://doi.org/10.1016/j.gca.2017.01.043

Bauch, D., Dmitrenko, I., Kirillov, S., Wegner, C., Hölemann, J., Pivovarov, S., et al. (2009). Eurasian Arctic shelf hydrography: Exchange and residence time of southern Laptev Sea waters. *Continental Shelf Research*, *29*(15), 1815–1820. https://doi.org/10.1016/j.csr.2009.06.009

Bauch, D., Schlosser, P., & Fairbanks, R. (1995). Freshwater balance and the sources of deep and bottom waters in the Arctic Ocean inferred from the distribution of $H_2{}^{18}O$. *Progress in Oceanography*, *35*, 53–80. https://doi.org/10.1016/0079-6611(95)00005-2

Beszczynska-Möller, A., Fahrbach, E., Schauer, U., & Hansen, E. (2012). Variability in Atlantic water temperature and transport at the entrance to the Arctic Ocean, 1997–2010. *ICES Journal of Marine Science*, *69*(5), 852–863. https://doi.org/10.1093/icesjms/fss056

Beszczynska-Möller, A., Woodgate, R., Lee, C., Melling, H., & Karcher, M. (2011). A synthesis of exchanges through the main oceanic gateways to the Arctic Ocean. *Oceanography*, *24*(3), 82–99. https://doi.org/10.5670/oceanog.2011.59

Bishop, J. K. B. (1988). The barite-opal-organic carbon association in oceanic particulate matter. *Nature*, *332*, 341–343. https://doi.org/10.1038/332341a0

Bolt, C. (2021). *Utility of trace element studies for improving our understanding of geochemical processes within the Arctic Ocean environment*. University of Alaska Fairbanks. Retrieved from https://books.google.com/books?id=Q5F8zgEACAAJ

Boyd, P. W., Claustre, H., Levy, M., Siegel, D. A., & Weber, T. (2019). Multi-faceted particle pumps drive carbon sequestration in the ocean. *Nature*, *568*, 9–335. https://doi.org/10.1038/s41586-019-1098-2

Bridgestock, L., Hsieh, Y.-T., Porcelli, D., Homoky, W. B., Bryan, A., & Henderson, G. M. (2018). Controls on the barium isotope compositions of marine sediments. *Earth and Planetary Science Letters*, *481*, 101–110. https://doi.org/10.1016/j.epsl.2017.10.019

Bridgestock, L., Nathan, J., Hsieh, Y.-T., Holdship, P., Porcelli, D., Andersson, P. S., & Henderson, G. M. (2021). Assessing the utility of barium isotopes to trace Eurasian riverine freshwater inputs to the Arctic Ocean. *Marine Chemistry*, *236*, 104029. https://doi.org/10.1016/j.marchem.2021.104029

Bridgestock, L., Nathan, J., Paver, R., Hsieh, Y.-T., Porcelli, D., Tanzil, J., et al. (2021). Estuarine processes modify the isotope composition of dissolved riverine barium fluxes to the ocean. *Chemical Geology*, *579*, 120340. https://doi.org/10.1016/j.chemgeo.2021.120340

Cao, Z., Rao, X., Yu, Y., Siebert, C., Hathorne, E. C., Liu, B., et al. (2021). Stable barium isotope dynamics during estuarine mixing. *Geophysical Research Letters*, *48*(19), e2021GL095680. https://doi.org/10.1029/2021GL095680

Cao, Z., Siebert, C., Hathorne, E. C., Dai, M., & Frank, M. (2020). Corrigendum to "Constraining the oceanic barium cycle with stable barium isotopes" [Earth Planet. Sci. Lett. 434 (2016) 1–9]. *Earth and Planetary Science Letters*, *530*, 116003. https://doi.org/10.1016/j.epsl.2019.116003

Cardinal, D., Savoye, N., Trull, T. W., André, L., Kopczynska, E. E., & Dehairs, F. (2005). Variations of carbon remineralisation in the Southern Ocean illustrated by the Baxs proxy. *Deep Sea Research Part I: Oceanographic Research Papers*, *52*(2), 355–370. https://doi.org/10.1016/j.dsr.2004.10.002

Carmack, E. C., Yamamoto-Kawai, M., Haine, T. W. N., Bacon, S., Bluhm, B. A., Lique, C., et al. (2016). Freshwater and its role in the Arctic marine system: Sources, disposition, storage, export, and physical and biogeochemical consequences in the Arctic and global oceans: Freshwater and the Arctic marine system. *Journal of Geophysical Research: Biogeosciences*, *121*(3), 675–717. https://doi.org/10.1002/2015JG003140

Chan, L. H., Drummond, D., Edmond, J. M., & Grant, B. (1977). On the barium data from the Atlantic GEOSECS expedition. *Deep Sea Research*, *24*(7), 613–649. https://doi.org/10.1016/0146-6291(77)90505-7

Charbonnier, Q., Moynier, F., & Bouchez, J. (2018). Barium isotope cosmochemistry and geochemistry. *Science Bulletin*, *63*(6), 385–394. https://doi.org/10.1016/j.scib.2018.01.018

Charette, M. A., Kipp, L. E., Jensen, L. T., Dabrowski, J. S., Whitmore, L. M., Fitzsimmons, J. N., et al. (2020). The transpolar drift as a source of riverine and shelf-derived trace elements to the central Arctic Ocean. *Journal of Geophysical Research: Oceans*, *125*(5). https://doi.org/10.1029/2019JC015920

Charette, M. A., Lam, P. J., Lohan, M. C., Kwon, E. Y., Hatje, V., Jeandel, C., et al. (2016). Coastal Ocean and shelf-sea biogeochemical cycling of trace elements and isotopes: Lessons learned from GEOTRACES. *Philosophical Transactions of the Royal Society A: Mathematical, Physical & Engineering Sciences*, *374*(2081), 20160076. https://doi.org/10.1098/rsta.2016.0076

Charkin, A. N., van der Loeff, M. R., Shakhova, N. E., Gustafsson, Ö., Dudarev, O. V., Cherepnev, M. S., et al. (2017). Discovery and characterization of submarine groundwater discharge in the Siberian Arctic seas: A case study in the Buor-Khaya Gulf, Laptev Sea. *The Cryosphere*, *11*(5), 2305–2327. https://doi.org/10.5194/tc-11-2305-2017

Chow, T. J., & Goldberg, E. D. (1960). On the marine geochemistry of barium. *Geochimica et Cosmochimica Acta*, *20*(3–4), 192–198. https://doi.org/10.1016/0016-7037(60)90073-9

Coachman, L. K., & Barnes, C. A. (1963). The movement of Atlantic water in the Arctic Ocean. *Arctic*, *16*(1), 1–80. https://doi.org/10.14430/arctic3517

Colbert, D., & McManus, J. (2005). Importance of seasonal variability and coastal processes on estuarine manganese and barium cycling in a Pacific Northwest estuary. *Continental Shelf Research*, *25*(11), 1395–1414. https://doi.org/10.1016/j.csr.2005.02.003

Colombo, M., Brown, K. A., De Vera, J., Bergquist, B. A., & Orians, K. J. (2019). Trace metal geochemistry of remote rivers in the Canadian Arctic Archipelago. *Chemical Geology*, *525*, 479–491. https://doi.org/10.1016/j.chemgeo.2019.08.006

Colombo, M., Jackson, S. L., Cullen, J. T., & Orians, K. J. (2020). Dissolved iron and manganese in the Canadian Arctic Ocean: On the biogeochemical processes controlling their distributions. *Geochimica et Cosmochimica Acta*, *277*, 150–174. https://doi.org/10.1016/j.gca.2020.03.012

Colombo, M., Rogalla, B., Myers, P. G., Allen, S. E., & Orians, K. J. (2019). Tracing dissolved lead sources in the Canadian Arctic: Insights from the Canadian GEOTRACES program. *ACS Earth and Space Chemistry*, *3*(7), 1302–1314. https://doi.org/10.1021/acsearthspacechem.9b00083

Crockford, P. W., Wing, B. A., Paytan, A., Hodgskiss, M. S. W., Mayfield, K. K., Hayles, J. A., et al. (2019). Barium-isotopic constraints on the origin of post-Marinoan barites. *Earth and Planetary Science Letters*, *519*, 234–244. https://doi.org/10.1016/j.epsl.2019.05.018

Cullen, J. T., & Sherrell, R. M. (1999). Techniques for determination of trace metals in small samples of size-fractionated particulate matter: Phytoplankton metals off central California. *Marine Chemistry*, *67*(3–4), 233–247. https://doi.org/10.1016/S0304-4203(99)00060-2

Cutter, G., Andersson, P. S., Codispoti, L. A., Croot, P., Francois, R., Lohan, M., et al. (2014). *Sampling and sample-handling protocols for GEOTRACES cruises, version 2*. Retrieved from http://www.geotraces.org/library-88/scientific-publications/reports/169-sampling-and-sample-handling-protocols-for-geotraces-cruises

Cutter, G., Kadko, D., & Landing, W. (2019). Bottle data from the GEOTRACES clean Carousel sampling system (GTC) on the Arctic section cruise (HLY1502) from August to October 2015 [Dataset Version 2019-07–29]. U.S. GEOTRACES Arctic Project. https://doi.org/10.1575/1912/bco-dmo.647259.4

De Baar, H. J. W., Timmermans, K. R., Laan, P., De Porto, H. H., Ober, S., Blom, J. J., et al. (2008). Titan: A new facility for ultraclean sampling of trace elements and isotopes in the deep oceans in the international geotraces program. *Marine Chemistry*, *111*(1–2), 4–21. https://doi.org/10.1016/j.marchem.2007.07.009

Dehairs, F., Chesselet, R., & Jedwab, J. (1980). Discrete suspended particles of barite and the barium cycle in the open ocean. *Earth and Planetary Science Letters*, *49*(2), 528–550. https://doi.org/10.1016/0012-821X(80)90094-1

Dehairs, F., Shopova, D., Ober, S., Veth, C., & Goeyens, L. (1997). Particulate barium stocks and oxygen consumption in the southern ocean mesopelagic water column during spring and early summer: Relationship with export production. *Deep Sea Research Part II: Topical Studies in Oceanography*, *44*(1–2), 497–516. https://doi.org/10.1016/S0967-0645(96)00072-0

Deng, N., Stack, A. G., Weber, J., Cao, B., De Yoreo, J. J., & Hu, Y. (2019). Organic–mineral interfacial chemistry drives heterogeneous nucleation of Sr-rich (Ba x, Sr $1-x$)SO 4 from undersaturated solution. *Proceedings of the National Academy of Sciences of the United States of America*, *116*(27), 13221–13226. https://doi.org/10.1073/pnas.1821065116

Dymond, J., Suess, E., & Lyle, M. (1992). Barium in deep-sea sediment: A geochemical proxy for paleoproductivity. *Paleoceanography and Paleoclimatology*, *7*(2), 163–181. https://doi.org/10.1029/92PA00181

Eagle, M., Paytan, A., Arrigo, K. R., van Dijken, G., & Murray, R. W. (2003). A comparison between excess barium and barite as indicators of carbon export. *Paleoceanography*, *18*(1), 1021. https://doi.org/10.1029/2002PA000793

Edmonds, H. N., Michael, P. J., Baker, E. T., Connelly, D. P., Snow, J. E., Langmuir, C. H., et al. (2003). Discovery of abundant hydrothermal venting on the ultraslow-spreading Gakkel Ridge in the Arctic Ocean. *Nature*, *421*(6920), 252–256. https://doi.org/10.1038/nature01351

Falkner, K. K., Macdonald, R. W., Carmack, E. C., & Weingartner, T. (2013). The potential of barium as a tracer of Arctic water masses. In O. M. Johannessen, R. D. Muench, & J. E. Overland (Eds.), *Geophysical monograph series* (pp. 63–76). American Geophysical Union. https://doi.org/10.1029/gm085p0063

Fransson, A., Chierici, M., Anderson, L. G., Bussmann, I., Kattner, G., Peter Jones, E., & Swift, J. H. (2001). The importance of shelf processes for the modification of chemical constituents in the waters of the Eurasian Arctic Ocean: Implication for carbon fluxes. *Continental Shelf Research*, *21*(3), 225–242. https://doi.org/10.1016/S0278-4343(00)00088-1

Gaillardet, J., Viers, J., & Dupré, B. (2014). Trace elements in river waters. In H. D.Holland & K. K.Turekian (Eds.), *Treatise on geochemistry* (pp. 195–235). Elsevier. https://doi.org/10.1016/B978-0-08-095975-7.00507-6

Ganeshram, R. S., François, R., Commeau, J., & Brown-Leger, S. L. (2003). An experimental investigation of barite formation in seawater. *Geochimica et Cosmochimica Acta*, *67*(14), 2599–2605. https://doi.org/10.1016/S0016-7037(03)00164-9

Geyman, B. M., Ptacek, J. L., LaVigne, M., & Horner, T. J. (2019). Barium in deep-sea bamboo corals: Phase associations, barium stable isotopes, & prospects for paleoceanography. *Earth and Planetary Science Letters*, *525*, 115751. https://doi.org/10.1016/j.epsl.2019.115751

Gong, D., & Pickart, R. S. (2016). Early summer water mass transformation in the eastern Chukchi Sea. *Deep Sea Research Part II: Topical Studies in Oceanography*, *130*, 43–55. https://doi.org/10.1016/j.dsr2.2016.04.015

Gou, L.-F., Jin, Z., Galy, A., Gong, Y.-Z., Nan, X.-Y., Jin, C., et al. (2020). Seasonal riverine barium isotopic variation in the middle Yellow River: Sources and fractionation. *Earth and Planetary Science Letters*, *531*, 115990. https://doi.org/10.1016/j.epsl.2019.115990

Granger, J., Sigman, D. M., Gagnon, J., Tremblay, J., & Mucci, A. (2018). On the properties of the Arctic halocline and deep water masses of the Canada Basin from nitrate isotope ratios. *Journal of Geophysical Research: Oceans*, *123*(8), 5443–5458. https://doi.org/10.1029/2018JC014110

Guay, C. K., & Falkner, K. K. (1997). Barium as a tracer of Arctic halocline and river waters. *Deep Sea Research Part II: Topical Studies in Oceanography*, *44*(8), 1543–1569. https://doi.org/10.1016/S0967-0645(97)00066-0

Guay, C. K., & Falkner, K. K. (1998). A survey of dissolved barium in the estuaries of major Arctic rivers and adjacent seas. *Continental Shelf Research*, *18*(8), 859–882. https://doi.org/10.1016/S0278-4343(98)00023-5

Guay, C. K., McLaughlin, F. A., & Yamamoto-Kawai, M. (2009). Differentiating fluvial components of upper Canada Basin waters on the basis of measurements of dissolved barium combined with other physical and chemical tracers. *Journal of Geophysical Research*, *114*. https://doi.org/10.1029/2008JC005099

Haine, T. W. N., Curry, B., Gerdes, R., Hansen, E., Karcher, M., Lee, C., et al. (2015). Arctic freshwater export: Status, mechanisms, and prospects. *Global and Planetary Change*, *125*, 13–35. https://doi.org/10.1016/j.gloplacha.2014.11.013

Hendry, K. R., Pyle, K. M., Barney Butler, G., Cooper, A., Fransson, A., Chierici, M., et al. (2018). Spatiotemporal variability of barium in Arctic sea-ice and seawater. *Journal of Geophysical Research: Oceans*, *123*(5), 3507–3522. https://doi.org/10.1029/2017JC013668

Ho, P., Shim, M. J., Howden, S. D., & Shiller, A. M. (2019). Temporal and spatial distributions of nutrients and trace elements (Ba, Cs, Cr, Fe, Mn, Mo, U, V and Re) in Mississippi coastal waters: Influence of hypoxia, submarine groundwater discharge, and episodic events. *Continental Shelf Research*, *175*, 53–69. https://doi.org/10.1016/j.csr.2019.01.013

Holmes, R. M., McClelland, J. W., Tank, S. E., Spencer, R. G. M., & Shiklomanov, A. I. (2018). Arctic great rivers observatory [Water Quality Dataset Version 20181010]. Woodwell Climate Research Center. Retrieved from https://www.arcticgreatrivers.org/data

Honjo, S., Krishfield, R. A., Eglinton, T. I., Manganini, S. J., Kemp, J. N., Doherty, K., et al. (2010). Biological pump processes in the cryopelagic and hemipelagic Arctic Ocean: Canada Basin and Chukchi Rise. *Progress in Oceanography*, *85*(3–4), 137–170. https://doi.org/10.1016/j.pocean.2010.02.009

Hoppema, M., Dehairs, F., Navez, J., Monnin, C., Jeandel, C., Fahrbach, E., & de Baar, H. J. W. (2010). Distribution of barium in the Weddell Gyre: Impact of circulation and biogeochemical processes. *Marine Chemistry*, *122*(1–4), 118–129. https://doi.org/10.1016/j.marchem.2010.07.005

Horner, T., & Crockford, P. (2021). *Barium isotopes: Drivers, dependencies, and distributions through space and time*. Cambridge University Press.

Horner, T. J., Kinsley, C. W., & Nielsen, S. G. (2015). Barium-isotopic fractionation in seawater mediated by barite cycling and oceanic circulation. *Earth and Planetary Science Letters*, *430*, 511–522. https://doi.org/10.1016/j.epsl.2015.07.027

Horner, T. J., Little, S. H., Conway, T. M., Farmer, J. R., Hertzberg, J. E., Janssen, D. J., et al. (2021). Bioactive trace metals and their isotopes as paleoproductivity proxies: An assessment using GEOTRACES-era data. *Global Biogeochemical Cycles*, *35*(11), e2020GB006814. https://doi.org/10.1029/2020GB006814

Hsieh, Y.-T., Bridgestock, L., Scheuermann, P. P., Seyfried, W. E., Jr., & Henderson, G. M. (2021). Barium isotopes in mid-ocean ridge hydrothermal vent fluids: A source of isotopically heavy Ba to the ocean. *Geochimica et Cosmochimica Acta*, *292*, 348–363. https://doi.org/10.1016/j.gca.2020.09.037

Hsieh, Y.-T., & Henderson, G. M. (2017). Barium stable isotopes in the global ocean: Tracer of Ba inputs and utilization. *Earth and Planetary Science Letters*, *473*, 269–278. https://doi.org/10.1016/j.epsl.2017.06.024

Hunkins, K., Thorndike, E. M., & Mathieu, G. (1969). Nepheloid layers and bottom currents in the Arctic Ocean. *Journal of Geophysical Research*, *74*(28), 6995–7008. https://doi.org/10.1029/JC074i028p06995

Hwang, J., Kim, M., Manganini, S. J., McIntyre, C. P., Haghipour, N., Park, J., et al. (2015). Temporal and spatial variability of particle transport in the deep Arctic Canada Basin: Particle flux in Canada Basin. *Journal of Geophysical Research: Oceans*, *120*(4), 2784–2799. https://doi.org/10.1002/2014JC010643

Jacquet, S. H. M., Dehairs, F., Cardinal, D., Navez, J., & Delille, B. (2005). Barium distribution across the southern ocean frontal system in the Crozet–Kerguelen basin. *Marine Chemistry*, *95*(3–4), 149–162. https://doi.org/10.1016/j.marchem.2004.09.002

Jakobsson, M. (2002). Hypsometry and volume of the Arctic Ocean and its constituent seas. *Geochemistry, Geophysics, Geosystems*, *3*(5), 1–18. https://doi.org/10.1029/2001GC000302

Jeandel, C., Peucker-Ehrenbrink, B., Jones, M. T., Pearce, C. R., Oelkers, E. H., Godderis, Y., et al. (2011). Ocean margins: The missing term in oceanic element budgets? *Eos*, *92*(26), 217–224. https://doi.org/10.1029/2011EO260001

Jensen, L. T., Wyatt, N. J., Twining, B. S., Rauschenberg, S., Landing, W. M., Sherrell, R. M., & Fitzsimmons, J. N. (2019). Biogeochemical cycling of dissolved zinc in the Western Arctic (Arctic GEOTRACES GN01). *Global Biogeochemical Cycles*, *33*(3), 343–369. https://doi.org/10.1029/2018GB005975

Jones, E. P., & Anderson, L. G. (1986). On the origin of the chemical properties of the Arctic Ocean halocline. *Journal of Geophysical Research*, *91*(C9), 10759. https://doi.org/10.1029/JC091iC09p10759

Kadko, D., Aguilar-Islas, A., Bolt, C., Buck, C. S., Fitzsimmons, J. N., Jensen, L. T., et al. (2019). The residence times of trace elements determined in the surface Arctic Ocean during the 2015 US Arctic GEOTRACES expedition. *Marine Chemistry*, *208*, 56–69. https://doi.org/10.1016/j.marchem.2018.10.011

Kipp, L. E., Charette, M. A., Moore, W. S., Henderson, P. B., & Rigor, I. G. (2018). Increased fluxes of shelf-derived materials to the central Arctic Ocean. *Science Advances*, *4*(1), eaao1302. https://doi.org/10.1126/sciadv.aao1302

Kipp, L. E., Henderson, P. B., Wang, Z. A., & Charette, M. A. (2020). Deltaic and estuarine controls on Mackenzie River solute fluxes to the Arctic Ocean. *Estuaries and Coasts*. https://doi.org/10.1007/s12237-020-00739-8

Kipp, L. E., Kadko, D. C., Pickart, R. S., Henderson, P. B., Moore, W. S., & Charette, M. A. (2019). Shelf-basin interactions and water mass residence times in the Western Arctic Ocean: Insights provided by radium isotopes. *Journal of Geophysical Research: Oceans*, *124*(5), 3279–3297. https://doi.org/10.1029/2019JC014988

Kipp, L. E., Spall, M. A., Pickart, R. S., Kadko, D. C., Moore, W. S., Dabrowski, J. S., & Charette, M. A. (2020). Observational and modeling evidence of seasonal trends in sediment-derived material inputs to the Chukchi sea. *Journal of Geophysical Research: Oceans*, *125*(5). https://doi.org/10.1029/2019JC016007

Klunder, M. B., Laan, P., Middag, R., de Baar, H. J. W., & Bakker, K. (2012). Dissolved iron in the Arctic Ocean: Important role of hydrothermal sources, shelf input and scavenging removal. *Journal of Geophysical Research: Oceans*, *117*, C04014. https://doi.org/10.1029/2011JC007135

Kondo, Y., Obata, H., Hioki, N., Ooki, A., Nishino, S., Kikuchi, T., & Kuma, K. (2016). Transport of trace metals (Mn, Fe, Ni, Zn and Cd) in the Western Arctic Ocean (Chukchi sea and Canada basin) in late summer 2012. *Deep Sea Research Part I: Oceanographic Research Papers*, *116*, 236–252. https://doi.org/10.1016/j.dsr.2016.08.010

Lalande, C., Forest, A., Barber, D. G., Gratton, Y., & Fortier, L. (2009). Variability in the annual cycle of vertical particulate organic carbon export on Arctic shelves: Contrasting the Laptev Sea, northern Baffin Bay and the Beaufort sea. *Continental Shelf Research*, *29*(17), 2157–2165. https://doi.org/10.1016/j.csr.2009.08.009

Lam, P. J. (2020). Size-fractionated major and minor particle composition and concentration from the US GEOTRACES Arctic cruise (HLY1502) on USCGC healy from August to October 2015 (Version 1). Biological and Chemical Oceanographic Data Management Office.

Lam, P. J., & Marchal, O. (2015). Insights into particle cycling from thorium and particle data. *Annual Review of Marine Science*, *7*(1), 159–184. https://doi.org/10.1146/annurev-marine-010814-015623

Laukert, G., Frank, M., Hathorne, E. C., Krumpen, T., Rabe, B., Bauch, D., et al. (2017). Pathways of Siberian freshwater and sea ice in the Arctic Ocean traced with radiogenic neodymium isotopes and rare earth elements. *Polarforschung*, *87*(1). https://doi.org/10.2312/POLARFORSCHUNG.87.1.3

LeBlond, P. H. (1980). On the surface circulation in some channels of the Canadian Arctic Archipelago. *Arctic*, *33*(1), 189–197. https://doi.org/10.14430/arctic2554

Lecher, A. L. (2017). Groundwater discharge in the Arctic: A review of studies and implications for biogeochemistry. *Hydrology*, *4*(3), 41. https://doi.org/10.3390/hydrology4030041

Lecher, A. L., Kessler, J., Sparrow, K., Garcia-Tigreros Kodovska, F., Dimova, N., Murray, J., et al. (2016). Methane transport through submarine groundwater discharge to the north Pacific and Arctic Ocean at two Alaskan sites: SGD methane transport. *Limnology & Oceanography*, *61*(S1), S344–S355. https://doi.org/10.1002/lno.10118

Lehmann, N., Kienast, M., Granger, J., Bourbonnais, A., Altabet, M. A., & Tremblay, J.-É. (2019). Remote western Arctic nutrients fuel remineralization in deep Baffin Bay. *Global Biogeochemical Cycles*, *33*(6), 649–667. https://doi.org/10.1029/2018GB006134

Lemaitre, N., Planchon, F., Planquette, H., Dehairs, F., Fonseca-Batista, D., Roukaerts, A., et al. (2018). High variability of particulate organic carbon export along the North Atlantic GEOTRACES section GA01 as deduced from 234Th fluxes. *Biogeosciences*, *15*(21), 6417–6437. https://doi.org/10.5194/bg-15-6417-2018

Le Roy, E., Sanial, V., Charette, M. A., van Beek, P., Lacan, F., Jacquet, S. H. M., et al. (2018). The 226Ra–Ba relationship in the north Atlantic during GEOTRACES-GA01. *Biogeosciences*, *15*(9), 3027–3048. https://doi.org/10.5194/bg-15-3027-2018

Manning, C., Bourbonnais, A., Granger, J., Hamme, R. C., Yeung, L., Amando Valerio, D., et al. (2020). *OB21B-05—Nitrogen cycling and circulation in Baffin Bay investigated with isotopic measurements of N2, N2O and NO3* [Presented at the Ocean Sciences Meeting]. AGU.

Marsay, C. M., Aguilar-Islas, A., Fitzsimmons, J. N., Hatta, M., Jensen, L. T., John, S. G., et al. (2018). Dissolved and particulate trace elements in late summer Arctic melt ponds. *Marine Chemistry*, *204*, 70–85. https://doi.org/10.1016/j.marchem.2018.06.002

Martinez-Ruiz, F., Paytan, A., Gonzalez-Muñoz, M. T., Jroundi, F., Abad, M. M., Lam, P. J., et al. (2019). Barite formation in the ocean: Origin of amorphous and crystalline precipitates. *Chemical Geology*, *511*, 441–451. https://doi.org/10.1016/j.chemgeo.2018.09.011

Mayfield, K. K., Eisenhauer, A., Santiago Ramos, D. P., Higgins, J. A., Horner, T. J., Auro, M., et al. (2021). Groundwater discharge impacts marine isotope budgets of Li, Mg, Ca, Sr, and Ba. *Nature Communications*, *12*(1), 148. https://doi.org/10.1038/s41467-020-20248-3

McClelland, J. W., Holmes, R. M., Dunton, K. H., & Macdonald, R. W. (2012). The Arctic Ocean estuary. *Estuaries and Coasts*, *35*(2), 353–368. https://doi.org/10.1007/s12237-010-9357-3

McLaughlin, F. A., Carmack, E. C., Ingram, R. G., Williams, W. J., & Michel, C. (2004). Chapter 31. Oceanography of the northwest passage (26,P). In A. R. Robinson, & K. H. Brink, (Eds.), *The global coastal ocean, Interdisciplinary regional studies and syntheses* (pp. 1211–1242). Harvard university Press.

McManus, J., Berelson, W. M., Klinkhammer, G. P., Johnson, K. S., Coale, K. H., Anderson, R. F., et al. (1998). Geochemistry of barium in marine sediments: Implications for its use as a paleoproxy. *Geochimica et Cosmochimica Acta*, *62*(21–22), 3453–3473. https://doi.org/10.1016/S0016-7037(98)00248-8

McManus, J., Berelson, W. M., Klinkhammer, G. P., Kilgore, T. E., & Hammond, D. E. (1994). Remobilization of barium in continental margin sediments. *Geochimica et Cosmochimica Acta*, *58*(22), 4899–4907. https://doi.org/10.1016/0016-7037(94)90220-8

Mears, C., Thomas, H., Henderson, P. B., Charette, M. A., MacIntyre, H., Dehairs, F., et al. (2020). Using 226Ra and 228Ra isotopes to distinguish water mass distribution in the Canadian Arctic Archipelago. *Biogeosciences*, *17*(20), 4937–4959. https://doi.org/10.5194/bg-17-4937-2020

Melling, H. (2000). Exchanges of freshwater through the shallow straits of the North American Arctic. In E. L. Lewis, E. P. Jones, P. Lemke, T. D. Prowse, (Eds.), *The freshwater budget of the Arctic Ocean* (pp. 479–502). Kluwer Academic Publishers.

Middag, R., de Baar, H. J. W., Laan, P., & Bakker, K. (2009). Dissolved aluminium and the silicon cycle in the Arctic Ocean. *Marine Chemistry*, *115*(3–4), 176–195. https://doi.org/10.1016/j.marchem.2009.08.002

Middag, R., de Baar, H. J. W., Laan, P., & Klunder, M. B. (2011). Fluvial and hydrothermal input of manganese into the Arctic Ocean. *Geochimica et Cosmochimica Acta*, *75*(9), 2393–2408. https://doi.org/10.1016/j.gca.2011.02.011

Millero, F. J. (1982). The effect of pressure on the solubility of minerals in water and seawater. *Geochimica et Cosmochimica Acta*, *46*(1), 11–22. https://doi.org/10.1016/0016-7037(82)90286-1

Milliman, J. D., & Farnsworth, K. L. (2013). *River discharge to the coastal ocean: A global synthesis*. Cambridge University Press.

Monnin, C., Jeandel, C., Cattaldo, T., & Dehairs, F. (1999). The marine barite saturation state of the world's oceans. *Marine Chemistry*, *65*(3–4), 253–261. https://doi.org/10.1016/S0304-4203(99)00016-X

Nancollas, G. H., & Purdie, N. (1963). Crystallization of barium sulphate in aqueous solution. *Transactions of the Faraday Society*, *59*, 735. https://doi.org/10.1039/tf9635900735

Newton, R., Schlosser, P., Mortlock, R., Swift, J., & MacDonald, R. (2013). Canadian basin freshwater sources and changes: Results from the 2005 Arctic Ocean section: AOS 2005 freshwater sources and changes. *Journal of Geophysical Research: Oceans*, *118*(4), 2133–2154. https://doi.org/10.1002/jgrc.20101

Nöthig, E.-M., Lalande, C., Fahl, K., Metfies, K., Salter, I., & Bauerfeind, E. (2020). Annual cycle of downward particle fluxes on each side of the Gakkel Ridge in the central Arctic Ocean. *Philosophical Transactions of the Royal Society A: Mathematical, Physical & Engineering Sciences*, *378*(2181), 20190368. https://doi.org/10.1098/rsta.2019.0368

Nurnberg, D. (1996). Biogenic barium and opal in shallow Eurasian shelf sediments in relation to the pelagic Arctic Ocean environment. *Reports on Polar Research*, *212*, 96–118.

Ober, S., Rijkenberg, M. J. A., & Gerringa, L. J. A. (2016). Physical oceanography measured with ultra clean CTD/Water sampler-system during POLARSTERN cruise PS94 (ARK-XXIX/3). Royal Netherlands Institute for Sea Research. https://doi.org/10.1594/PANGAEA.859560

Ohnemus, D. C., Auro, M. E., Sherrell, R. M., Lagerström, M., Morton, P. L., Twining, B. S., et al. (2014). Laboratory intercomparison of marine particulate digestions including Piranha: A novel chemical method for dissolution of polyethersulfone filters. *Limnology and Oceanography: Methods*, *12*(8), 530–547. https://doi.org/10.4319/lom.2014.12.530

Peterson, I., Hamilton, J., Prinsenberg, S., & Pettipas, R. (2012). Wind-forcing of volume transport through Lancaster Sound: Transport through Lancaster Sound. *Journal of Geophysical Research: Oceans*, *117*(C11018). https://doi.org/10.1029/2012JC008140

Planquette, H., & Sherrell, R. M. (2012). Sampling for particulate trace element determination using water sampling bottles: Methodology and comparison to in situ pumps: Particulate trace element sampling. *Limnology and Oceanography: Methods*, *10*(5), 367–388. https://doi.org/10.4319/lom.2012.10.367

Prinsenberg, S., Hamilton, J., Peterson, I., & Pettipas, R. (2009). Observing and interpreting the seasonal variability of the oceanographic fluxes passing through Lancaster Sound of the Canadian Arctic Archipelago. In J. C. J. Nihoul & A. G. Kostianoy (Eds.), *Influence of climate change on the changing Arctic and sub-Arctic conditions* (pp. 125–143). Springer. https://doi.org/10.1007/978-1-4020-9460-6_10

R Core Team. (2018). R: A language and environment for statistical computing. R foundation for Statistical Computing.

Rember, R. (2018). Dissolved barium measured on water bottle samples during POLARSTERN cruise PS94 (ARK-XXIX/3) to the central Arctic ocean (Vol. 2015). PANGAEA. https://doi.org/10.1594/PANGAEA.896022

Roeske, T., Bauch, D., van der Loeff, M. R., & Rabe, B. (2012). Utility of dissolved barium in distinguishing north American from Eurasian runoff in the Arctic Ocean. *Marine Chemistry*, *132*(133), 1–14. https://doi.org/10.1016/j.marchem.2012.01.007

Roeske, T., Rutgers van der Loeff, M., Middag, R., & Bakker, K. (2012). Deep water circulation and composition in the Arctic Ocean by dissolved barium, aluminium and silicate. *Marine Chemistry*, *132*(133), 56–67. https://doi.org/10.1016/j.marchem.2012.02.001

Rudels, B. (1986). The outflow of polar water through the Arctic Archipelago and the oceanographic conditions in Baffin Bay. *Polar Research*, *4*(2), 161–180. https://doi.org/10.3402/polar.v4i2.6929

Rudels, B. (2015). Arctic Ocean circulation, processes and water masses: A description of observations and ideas with focus on the period prior to the international polar year 2007–2009. *Progress in Oceanography*, *132*, 22–67. https://doi.org/10.1016/j.pocean.2013.11.006

Rudels, B. (2018). Arctic Ocean circulation. In J. K. Cochran, H. Bokuniewicz, & P. Yager (Eds.), *Encyclopedia of Ocean Sciences* (pp. 1–16). Elsevier. https://doi.org/10.1016/B978-0-12-409548-9.11209-6

Rudels, B., Jones, E. P., Schauer, U., & Eriksson, P. (2004). Atlantic sources of the Arctic Ocean surface and halocline waters. *Polar Research*, *23*(2), 181–208. https://doi.org/10.3402/polar.v23i2.6278

Rudels, B., & Quadfasel, D. (1991). Convection and deep water formation in the Arctic Ocean-Greenland Sea system. *Journal of Marine Systems*, *2*(3–4), 435–450. https://doi.org/10.1016/0924-7963(91)90045-V

Rudnick, R. L., & Gao, S. (2014). 4.1—Composition of the continental crust. In H. D. Holland & K. K. Turekian (Eds.), *Treatise on geochemistry* (2nd ed., pp. 1–51). Elsevier.

Rushdi, A. I., McManus, J., & Collier, R. W. (2000). Marine barite and celestite saturation in seawater. *Marine Chemistry*, *69*(1–2), 19–31. https://doi.org/10.1016/S0304-4203(99)00089-4

Schauer, U. (1995). The release of brine-enriched shelf water from Storfjord into the Norwegian Sea. *Journal of Geophysical Research*, *100*(C8).

Schlitzer, R. (2018). Ocean data view 5.1.5. Retrieved from https://odv.awi.de

Schlitzer, R., Anderson, R. F., & Masferrer Dodas, E. (2018). The GEOTRACES intermediate data product 2017. *Chemical Geology*. https://doi.org/10.1016/J.CHEMGEO.2018.05.040

Schlosser, P., Bayer, R., Bönisch, G., Cooper, L. W., Ekwurzel, B., Jenkins, W. J., et al. (1999). Pathways and mean residence times of dissolved pollutants in the ocean derived from transient tracers and stable isotopes. *The Science of the Total Environment*, *237–238*, 15–30. https://doi.org/10.1016/S0048-9697(99)00121-7

Schlosser, P., Swift, J. H., Lewis, D., & Pfirman, S. L. (1995). The role of the large-scale Arctic Ocean circulation in the transport of contaminants. *Deep Sea Research Part II: Topical Studies in Oceanography*, *42*(6), 1341–1367. https://doi.org/10.1016/0967-0645(95)00045-3

Shaw, T. J., Moore, W. S., Kloepfer, J., & Sochaski, M. A. (1998). The flux of barium to the coastal waters of the southeastern USA: The importance of submarine groundwater discharge. *Geochimica et Cosmochimica Acta*, *62*(18), 3047–3054. https://doi.org/10.1016/S0016-7037(98)00218-X

Shiller, A., & Horner, T. (2021). Dissolved Ba, Cd, Cu, Ga, Mn, Ni, and V concentrations and Ba isotope concentrations from the US GEOTRACES Arctic expedition (GN01, HLY1502) from August to October 2015 (Version 3). Biological and Chemical Oceanography Data Management Office. https://doi.org/10.1575/1912/bco-dmo.772645.1

Spall, M. A. (2007). Circulation and water mass transformation in a model of the Chukchi Sea. *Journal of Geophysical Research*, *112*(C5), C05025. https://doi.org/10.1029/2005JC003364

Steele, M., Morison, J., Ermold, W., Rigor, I., Ortmeyer, M., & Shimada, K. (2004). Circulation of summer Pacific halocline water in the Arctic Ocean. *Journal of Geophysical Research*, *109*, C02027. https://doi.org/10.1029/2003JC002009

Talley, L. D., Pickard, G. L., Emery, W. J., & Swift, J. H. (2011). Arctic Ocean and Nordic seas. In L. D. Talley, (Eds.), *Descriptive physical Oceanography* (pp. 401–436). Elsevier. https://doi.org/10.1016/B978-0-7506-4552-2.10012-5

Tanhua, T., Jones, E. P., Jeansson, E., Jutterström, S., Smethie, W. M., Wallace, D. W. R., & Anderson, L. G. (2009). Ventilation of the Arctic Ocean: Mean ages and inventories of anthropogenic CO 2 and CFC-11. *Journal of Geophysical Research*, *114*(C1), C01002. https://doi.org/10.1029/2008JC004868

Taylor, J. R., Falkner, K. K., Schauer, U., & Meredith, M. (2003). Quantitative considerations of dissolved barium as a tracer in the Arctic Ocean. *Journal of Geophysical Research*, *108*(C12), 3374. https://doi.org/10.1029/2002JC001635

Thomas, H., Mucci, A., Mears, C., Charette, M. A., & Dehairs, F. (2021). Inorganic carbon, Ra, Ba and, δ18O tracer distribution in the Canadian Arctic Archipelago from the 2015 Canadian GEOTRACES expedition. PANGAEA. https://doi.org/10.1594/PANGAEA.929298

Thomas, H., Shadwick, E., Dehairs, F., Lansard, B., Mucci, A., Navez, J., et al. (2011). Barium and carbon fluxes in the Canadian Arctic Archipelago. *Journal of Geophysical Research*, *116*, C00G08. https://doi.org/10.1029/2011JC007120

Timmermans, M.-L., Proshutinsky, A., Golubeva, E., Jackson, J. M., Krishfield, R., McCall, M., et al. (2014). Mechanisms of Pacific summer water variability in the Arctic's central Canada Basin. *Journal of Geophysical Research: Oceans*, *119*(11), 7523–7548. https://doi.org/10.1002/2014JC010273

Top, Z., Clarke, W. B., Eismont, W. C., & Jones, E. P. (1980). Radiogenic helium in Baffin Bay bottom water. *Journal of Marine Research*, *38*, 435–452.

von Allmen, K., Böttcher, M. E., Samankassou, E., & Nägler, T. F. (2010). Barium isotope fractionation in the global barium cycle: First evidence from barium minerals and precipitation experiments. *Chemical Geology*, *277*(1–2), 70–77. https://doi.org/10.1016/j.chemgeo.2010.07.011

Wassmann, P., Duarte, C. M., Agustí, S., & Sejr, M. K. (2011). Footprints of climate change in the Arctic marine ecosystem. *Global Change Biology*, *17*(2), 1235–1249. https://doi.org/10.1111/j.1365-2486.2010.02311.x

Weingartner, T. J., Cavalieri, D. J., Aagaard, K., & Sasaki, Y. (1998). Circulation, dense water formation, and outflow on the northeast Chukchi Shelf. *Journal of Geophysical Research: Oceans*, *103*(C4), 7647–7661. https://doi.org/10.1029/98JC00374

Whitmore, L. M., Morton, P. L., Twining, B. S., & Shiller, A. M. (2019). Vanadium cycling in the Western Arctic Ocean is influenced by shelf-basin connectivity. *Marine Chemistry*, *216*, 103701. https://doi.org/10.1016/j.marchem.2019.103701

Whitmore, L. M., Pasqualini, A., Newton, R., & Shiller, A. M. (2020). Gallium: A new tracer of Pacific water in the Arctic Ocean. *Journal of Geophysical Research: Oceans*, *125*(7). https://doi.org/10.1029/2019JC015842

Woodgate, R. A., Weingartner, T. J., & Lindsay, R. (2012). Observed increases in Bering Strait oceanic fluxes from the Pacific to the Arctic from 2001 to 2011 and their impacts on the Arctic Ocean water column. *Geophysical Research Letters*, *39*(24), 2012GL054092. https://doi.org/10.1029/2012GL054092

Xiang, Y., & Lam, P. J. (2020). Size-fractionated marine suspended particle dynamics in the Western Arctic Ocean: Lateral and vertical sources. *Journal of Geophysical Research: Oceans*, *125*(8), e2020JC016144.

Yamamoto-Kawai, M., Carmack, E. C., McLaughlin, F. A., & Falkner, K. K. (2010). Oxygen isotope ratio, barium and salinity in waters around the North American coast from the Pacific to the Atlantic: Implications for freshwater sources to the Arctic throughflow. *Journal of Marine Research*, *68*(1), 97–117. https://doi.org/10.1357/002224010793078988